THE ASTROPHYSICAL JOURNAL, 272:509–539, 1983 September 15

NEUTRAL INTERSTELLAR GAS IN THE LOWER GALACTIC HALO

C. E. ALBERT
Yerkes Observatory, University of Chicago
Received 1982 July 12; accepted 1983 February 23

ABSTRACT

Optical interstellar absorption lines of Ti II, Ca II, and Na I, and the 21 cm emission line of H I have been observed at high resolution and high detection sensitivity toward nine pairs of nearly aligned distant halo stars and foreground disk stars with well-determined distances. Analysis of the column densities, velocities, and the directly determined variation of the titanium abundances with z-distance leads to a general picture of the neutral interstellar material in the lower galactic halo. Two types of gas with distinct distribution, kinematics, and abundances are found: a thick, low-velocity disk (type A) extending from the plane to well beyond the thin disk of OB stars, and a high-velocity, much less strongly depleted gas (type B) observed only at high z-distances, which constitutes at least 24% of the mass of the halo gas. The observed velocity distribution does not agree well with that predicted by a model corotating halo. The possible origins of the observed gas and its connection with QSO absorption lines are discussed.

Subject headings: galaxies: Milky Way — galaxies: structure — interstellar: matter — quasars

I. INTRODUCTION

The study of the interstellar medium in the galactic halo is a relatively new subject. Unlike the well-observed regions of the disk in the solar neighborhood, the halo poses a fundamental problem to absorption-line studies in the form of a crucial scarcity of useful background sources at high galactic latitude. Three investigations, in particular, can be cited as major advances in this subject: the pioneering work of Münch and Zirin (1961, hereafter MZ) two decades ago, which forms the classic set of optical absorption-line measurements toward high-latitude OB stars, and the more recent observations of ultraviolet and optical absorption lines formed toward a large number of extragalactic sources carried out by Savage and de Boer (1981) and by Songaila and York (1980), respectively.

MZ measured the velocities and visual intensities of the Ca II interstellar absorption lines toward a sample of 24 stars, most with spectral types taken from Morgan, Code, and Whitford (1955) which yielded z-distances ranging from 200 pc to beyond 2 kpc. From these observations, they concluded that there is a real increase with distance in the number of Ca II components per star, and therefore, that some of the observed gas must be located at distances up to a kiloparsec from the galactic plane. These indications of interstellar clouds well outside the plane prompted Spitzer (1956) to propose a hot galactic corona as a confining medium for the cool clouds.

Currently, interest in the halo has intensified along two fronts: the necessity of understanding both the basic structure of our own Galaxy and the origin of QSO absorption lines. A galactic corona could play a major role in the overall dynamics of our Galaxy, perhaps forming a galactic wind (Chevalier and Oegerle 1979; Bregman 1980*a*) or interacting with disk gas through a galactic fountain (Shapiro and Field 1976; Bregman 1980*b*). Further, if the halo contains sufficient material, and if such halos are typical of spiral galaxies, a superposition of intervening galaxies along the lines of sight to distant QSOs could produce the various red-shifted absorption-line systems commonly observed in their spectra (Bahcall and Spitzer 1969; Sargent *et al.* 1979; Savage and Jeske 1981). To investigate these possibilities, the full extent and amount of halo material in our Galaxy must be probed, a result most directly accomplished by observing along lines of sight to very distant sources. At ultraviolet wavelengths, Savage and de Boer have observed, toward nine stars in the Magellanic Clouds, both cool, mostly neutral gas in the form of absorption by such ions as C II, Si II, and Fe II and warm, ionized gas characterized by strong C IV and Si IV absorption. Although the detailed interpretation of these observations is complex, it appears clear that, compared with generally weak C IV and Si IV absorption seen toward nearby stars (Black *et al.* 1980; Cowie, Taylor, and York 1981), strong high-ion absorption toward the extragalactic stars is produced primarily by more distant gas within the galactic halo (Pettini and West 1982). The largest group of recent optical observations has been compiled by Songaila and York and consists of high-resolution spectra of galactic Ca II and Na I absorption toward four globular cluster cores, 11

LMC and SMC supergiants, three Seyfert galaxy nuclei, and the quasar 3C 273. Along many different paths through the galactic halo, they detect one unambiguous halo cloud, to within a sensitivity limit of about 30 mÅ at velocities $|v| \geq 30$ km s^{-1} at the K line.

It is obviously extremely important to have sampled the entire path length through the galactic halo. Nonetheless, a recent study of interstellar H I derived from observations of both the Lyα absorption line and the 21 cm emission line toward 10 of the OB stars originally observed by MZ demonstrates that the cold interstellar gas producing optical and Lyα absorption lines is located almost entirely in the lower ($|z| < 2$ kpc) regions of the halo (Hobbs *et al.* 1982, hereafter HMAL). The goal of the present work is an analysis of the physical and kinematic properties of this interstellar gas in the lower halo, where we are able to study at high sensitivity and resolution the detailed velocity structure of small amounts of absorbing material. The observations along each line of sight include the Ti II line at 3383.761 Å, the K line of Ca II, the D lines of Na I, and the 21 cm emission line of H I. Three features of these observations distinguish them from previous work. First, explicit limits can be placed on the distance to each cloud by comparing the absorption lines formed toward nearly aligned pairs of foreground and background stars with well-determined distances. Second, the optical velocity resolution of 5 km s^{-1} represents a gain by factors of 2–5 over the previously described work and, along with the good photometric accuracy achieved, allows both a detection limit about 10 times more sensitive than that of Songaila and York, for example, and the more detailed study of resolved, individual interstellar clouds. Finally, the λ3384 absorption line of Ti II is a uniquely accurate probe of interstellar depletion in each cloud. As Wallerstein and Goldsmith (1974) emphasized, the almost exact coincidence of the ionization potentials of Ti II and H I ensures that Ti II is the dominant ionization stage in H I regions. In addition, the weak λ3384 line generally remains optically thin. Thus, unlike the widely observed ions of Ca II and Na I, for example, for which somewhat uncertain ionization and line-saturation corrections are required, titanium abundances are observed directly and accurately. From observations of Ti II and the 21 cm emission line of neutral hydrogen, it is thus possible to determine the depletion of the interstellar gas above the galactic plane.

II. OBSERVATIONS AND REDUCTIONS

To study the lower galactic halo, lines of sight were selected toward early-type stars with $V \leq 7.5$, $|b| > 30°$, and $|z| > 500$ pc. A sample of nine suitable stars was chosen from the lists of Morgan, Code, and Whitford (1955), MZ, Hill (1970), Rickard (1972), and Cohen (1974). The most difficult step in this selection was obtaining reliable distances to these high-latitude stars. The problem caused by similarities between the spectra of young, massive, luminous Population I OB stars and evolved, low-mass, faint Population II stars in the same effective temperature range was recognized by MZ and has been actively discussed in the literature (Tobin and Kilkenny 1981; Walborn 1983). Accordingly, Dr. W. W. Morgan very kindly has determined accurate new spectral types for the program stars in this study, on the revised MK system defined in the *Spectral Atlas* of Morgan, Abt, and Tapscott (1978). Spectroscopic parallaxes were calculated from the new MK types, using intrinsic colors from Johnson (1963) and absolute magnitudes from Blaauw (1963) and correcting the apparent magnitudes for interstellar extinction with $A_V/E(B-V) = 3$; the resulting distances may be reliable to within about 25%.

The spectra of all of the program stars appear normal in comparison with Population I MK standards. Only one star, HD 93521, has been regarded as a possible subdwarf (Bisiacchi *et al.* 1978; Ramella, Morossi, and Santin 1980), and its spectrum is reproduced and discussed in comparison with both Population I standards and a well-known subdwarf by HMAL. Further, the number of field Population II "UV bright" stars expected to contaminate the present sample can be estimated by applying, to the number of field RR Lyrae stars satisfying the above selection criteria, the ratio of such stars known in globular clusters to cluster RR Lyrae stars. In five globular clusters whose memberships are well determined from proper motion studies (Cudworth 1976*a*, *b*, 1979*a*, *b*, *c*, *d*), the ratio of the total number of "UV bright" stars (Zinn, Newell, and Gibson 1972) to the total number of RR Lyrae stars (Hogg 1973) is 1/61. With the selection criteria of the present study, it is roughly estimated that 16 field RR Lyrae stars (Preston 1959) could be observed. Thus, no "UV bright" star is statistically expected to contaminate the observed sample.

Since it is important to separate out as effectively as possible the absorption arising locally in the disk along the observed lines of sight, foreground stars lying at small angular separations from the respective distant stars were chosen from the *Catalogue of Bright Stars* (Hoffleit 1964). The final observing list consisted of nine lines of sight toward eight pairs and one triplet of nearly aligned stars. The 19 stars observed are described in Table 1. For each pair of background (halo) and foreground (disk) stars, the separation is given both in degrees and as the projected linear separation, in parsecs, at the distance of the foreground star. The galactic coordinates of each line of sight are plotted in Figure 1. As indicated in Table 1, all of the background halo stars and two of the foreground disk stars of the present sample were included in the survey of MZ. In addition, the line of sight toward HD 93521 has been studied in detail by Caldwell (1979).

The observations were made with the echelle grating of the coudé spectrograph at the 2.7 m telescope of

TABLE 1

THE STARS OBSERVED

STAR	l	b	SEPARATION deg	SEPARATION pc	SP. TYPE	REFS.	V	$(B-V)$	REFS.	E_{B-V}	d(pc)	z(pc)	v_{LSR} (km s^{-1})	REFS.	$v \sin i$ (km s^{-1})	REFS.
HD 93521	183°1	+62°2	...	...	O9.5 V	1	7.04	−0.28	5	0.02	2100	1800	−13	10	400	12
32 LMi	182.0	+58.4	3.8	12	A4 IV	2	5.87	+0.07	2,6	0.00	170	150	+5	11	70	13
HD 97991	262.3	+51.7	...	...	B1.5 V	1	7.42	−0.24	6	0.01	1200	1000	+20	10	170	13
69 Leo	258.1	+54.1	3.5	5.0	A0 V	3	5.42	−0.03	7	0.00	80	65	+1	11	177	13
HD 119608	320.4	+43.1	...	...	B1 Ib	1	7.56	−0.08	5	0.11	3900	2600	+25	10	55:	13
85 Vir	321.6	+45.1	2.2	4.9	A2 Vn	3	6.19	+0.05	6	0.00	100	70	−38	11	...	...
HD 149881	31.4	+36.2	...	...	B0.5 II	1	7.03	−0.19	5	0.07	2500	1500	+30	10	...	...
HD 150483	29.5	+34.5	4.6	7.2	A2 V	2	5.94	+0.05	2,6	0.00	90	50	−11	11	230	13
18 Peg	65.8	−36.5	...	...	B3 III	1	6.00	−0.12	7	0.08	500	−300	+3	10	...	...
π Aqr	66.0	−44.8	8.3	52	B1 Ve	4	4.64	−0.04	7	0.22	330	−230	−3	10	278	13
HD 214080	44.8	−56.9	...	...	B1 Ib	1	6.80	−0.14	8	0.05	3000	−2500	+3	10	102	13,14
35 Aqr	37.1	−51.8	6.7	54	B2.5 IV	4	5.74	−0.15	2,9	0.07	460	−360	−1	10	...	...
HD 215733	85.2	−36.4	...	...	B1 II	1	7.32	−0.14	5	0.10	2500	−1500	−14	10	67:	13
HD 214930	88.3	−30.1	6.8	120	B2 IV	5	7.38	−0.14	5	0.10	1200	−600	−43	10	0	13
31 Peg	75.3	−36.4	8.0	34	B2 V	1	4.99	−0.10	7	0.14	260	−150	+19	11	134	13
HD 219188	83.0	−50.2	...	...	B0.5 Ib–IIn?	1	6.93	−0.18	9	0.06	2800?	−2200?	+53	10	185	13
58 Peg	85.8	−45.6	4.9	13	B9 III	3	5.38	−0.08	6	0.00	160	−110	+15	11	172:	13
HD 220172	68.1	−62.7	...	...	B2 V:	1	7.66	−0.20	5	0.04	1000	−900	+14	10	...	...
ψ^2 Aqr	67.6	−61.6	1.1	2.7	B5 V	2	4.40	−0.14	7	0.02	140	−120	−4	11	331	13

REFERENCES.—(1) W. W. Morgan 1981, private communication. (2) Hoffleit 1964. (3) Cowley *et al.* 1969. (4) Lesh 1968. (5) Guetter 1974. (6) Blanco *et al.* 1968. (7) Johnson *et al.* 1966. (8) Hill 1970. (9) Bohlin, Savage, and Drake 1978. (10) MZ. (11) Wilson 1953. (12) Conti and Ebbets 1977. (13) Uesugi and Fukuda 1970. (14) Tobin and Kilkenny 1981.

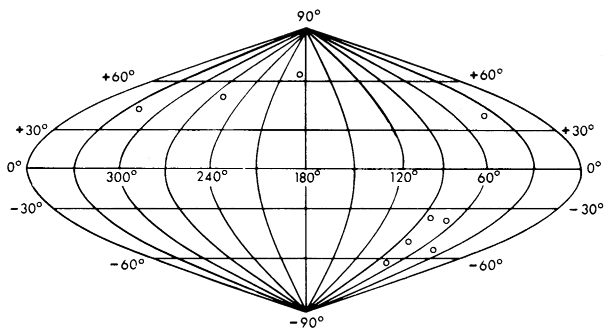

FIG. 1.—Galactic coordinates of observed lines of sight

McDonald Observatory in 1980 April and October and 1981 April and October. The detector was a self-scanned Digicon (Tull, Choisser, and Snow 1975; Vogt, Tull, and Kelton 1978), in which two linear arrays of 936 silicon photodiodes are preceded by a magnetically focused image intensifier tube with an S-20 photocathode. Instrumental backgrounds are automatically subtracted by magnetically deflecting the photoelectrons from one array to the other for photon-noise–limited integrations, typically of 30 s each. A complete exposure then consists of two independent spectra, each co-added from many such short integrations. Toward each star, the interstellar absorption lines of Ti II λ3383.761, Ca II λ3933.663, Na I $\lambda\lambda$5889.953 and 5895.923, and, in a few cases, Na I $\lambda\lambda$3302.369 and 3302.979 were recorded at resolutions (FWHM) of, respectively, 0.06, 0.07, 0.12, and 0.06 Å, corresponding to velocity resolutions of 5.5, 5.4, 5.9, and 5.2 km s^{-1}. Wavelength scales were established by repeated exposures of titanium, calcium, and sodium hollow-cathode lamps, and each spectrum was divided by a high-precision white lamp exposure to remove the instrumental response function. The resulting spectra are presented in Figure 2. The small triangles on the velocity axes represent the zero points of the heliocentric velocity scales, while the plotted LSR velocities were determined for the standard solar motion of 20 km s^{-1} toward $\alpha(1900) = 18^{h}$ and $\delta(1900) = 30°$. Stellar K lines are evident in the Ca II spectra toward 32 LMi, 18 Peg, 35 Aqr, HD 214930, and HD 220172 and are indicated by curvature in the respective continua from which the interstellar equivalent widths were measured. Absorption lines from telluric water vapor frequently contaminate the spectral region of the D lines (Hobbs 1978*b*) and are identified by tick marks above the continua; where coincident with interstellar lines, their contribution has been subtracted from the measured line strength.

The equivalent widths were obtained directly from the observations in the standard manner:

$$W_{\lambda} = \Delta\lambda \sum_{i=1}^{N_L} (1 - r_i), \qquad (1)$$

where N_L is the number of data points in the line, r_i is the residual intensity at wavelength λ_i, and $\Delta\lambda$ is the wavelength interval. The one-sigma errors in the equivalent widths were computed as described by Stokes (1978), as the sum of errors in the residual intensity, continuum placement, and wavelength interval. In all cases of this study, the dominant source of error is the first of these three, viz., the photon shot noise calculated as the standard deviation of all of the individual independent measurements of the residual intensity about their respective means. It is this uncertainty that determines the fundamental detection limit of each spectrum, which averaged 4, 4, and 6 mÅ for the lines of Ti II, Ca II, and Na I, respectively. For weak, unsaturated lines, the relation characterizing the linear part of the curve-of-growth was employed to calculate straightforwardly the column density of each line from its equivalent width. For lines of increasing strength, it rapidly becomes necessary to correct for the effects of saturation (Nachman and Hobbs 1973). For such strong lines, column densities were determined from a least squares profile-fitting program which uses techniques of Vidal-Madjar, Laurent, and Bonnet (1977) and York (1983). A theoretical absorption-line profile for a multicomponent line is calculated from a series expansion of the Voigt function and convolved with a Gaussian instrumental profile. Three parameters, column density, line-width b, and radial velocity, can be varied to achieve the best fit of the model to the observed line profile. Initial values for the fitting process were estimated from the linear curve-of-growth for each ion. Both the curve-of-growth and the profile-fitting methods are of course inherently limited by the assumed velocity distribution of the absorbers and by the choice of the number of line components apparent for a given instrumental resolution. Oscillator strengths were taken from Morton and Smith (1973). Table 2 lists the total observed equivalent widths and calculated column densities integrated over the entire velocity range toward each star. Only lower limits on the derived column density are quoted where the line is affected strongly by saturation. In one case, the line of sight toward 32 LMi, further consideration of the relatively noisy Ti II spectrum has resulted in a modification of the preliminary results reported by Albert (1982, hereafter Paper I), with the equivalent widths now better represented by an upper limit.

Along each line of sight, the total absorption profile can be divided into separate kinematic components, or clouds, and Table 3 compiles the observed equivalent widths and the calculated column densities for such individual clouds, identified by their LSR velocity. In some cases where the column densities were determined by the profile-fitting process, the integrated equivalent width was allocated among the individual blended line components in proportions slightly different from those derived from the visual inspection used to define the

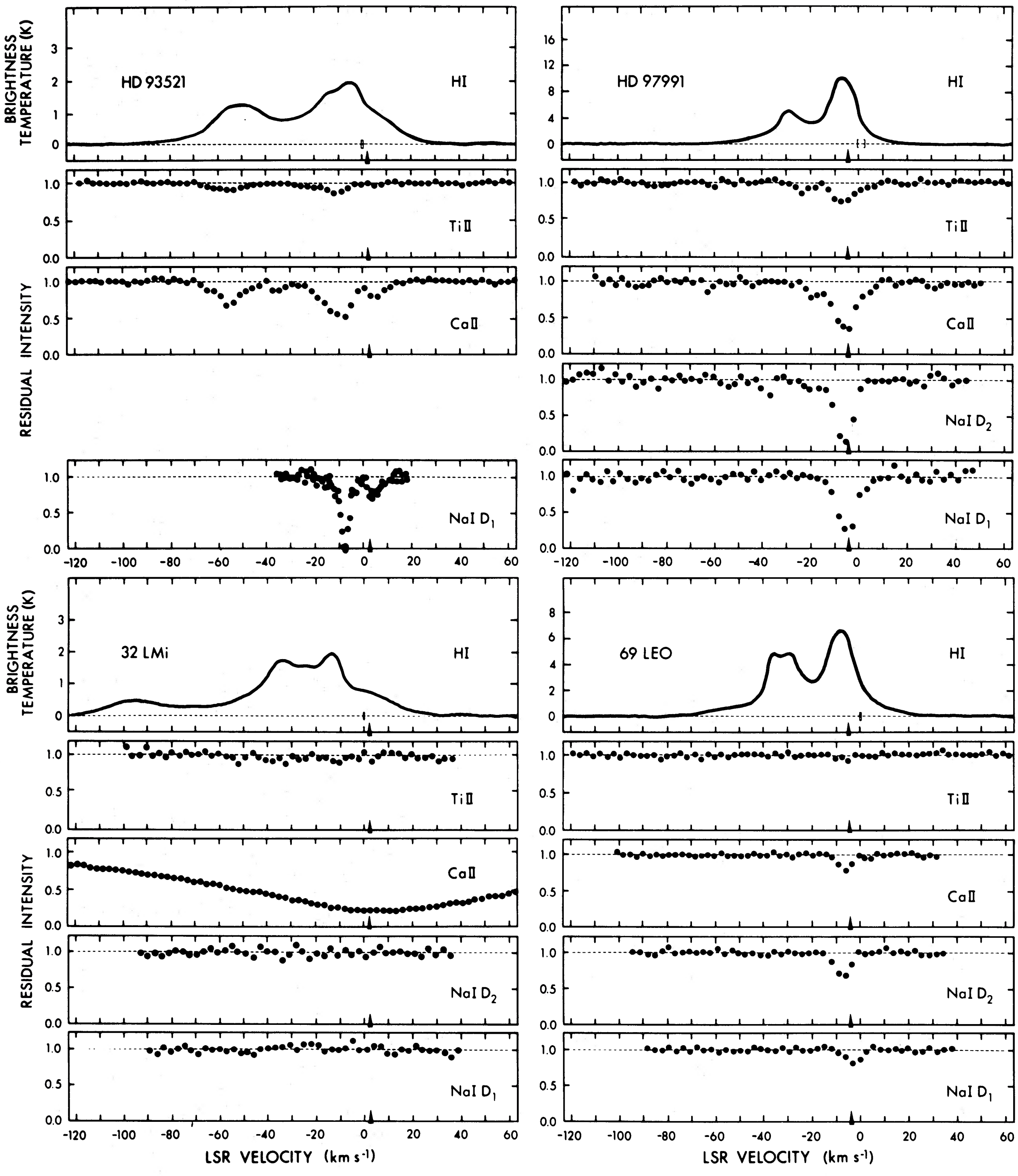

FIG. 2.—The interstellar absorption lines of Ti II, Ca II, Na I, and the H I 21 cm emission line along nine high-latitude lines of sight toward pairs of background halo stars and nearly aligned foreground disk stars. The velocity scale and stellar and telluric absorption lines are discussed in the text. The Na I D_1 scan toward HD 93521 is from Hobbs (1978*a*).

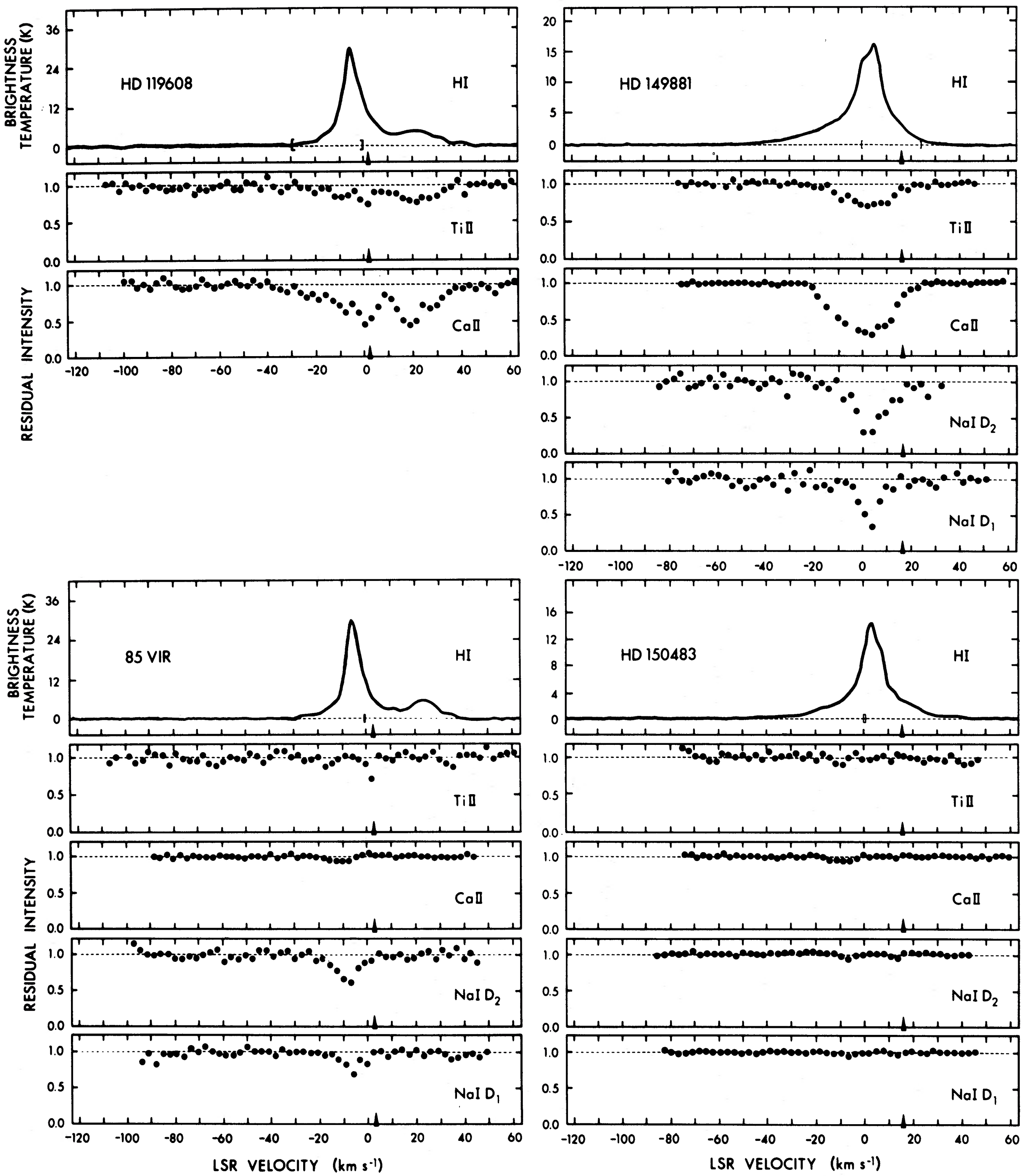

FIG. 2—*Continued*

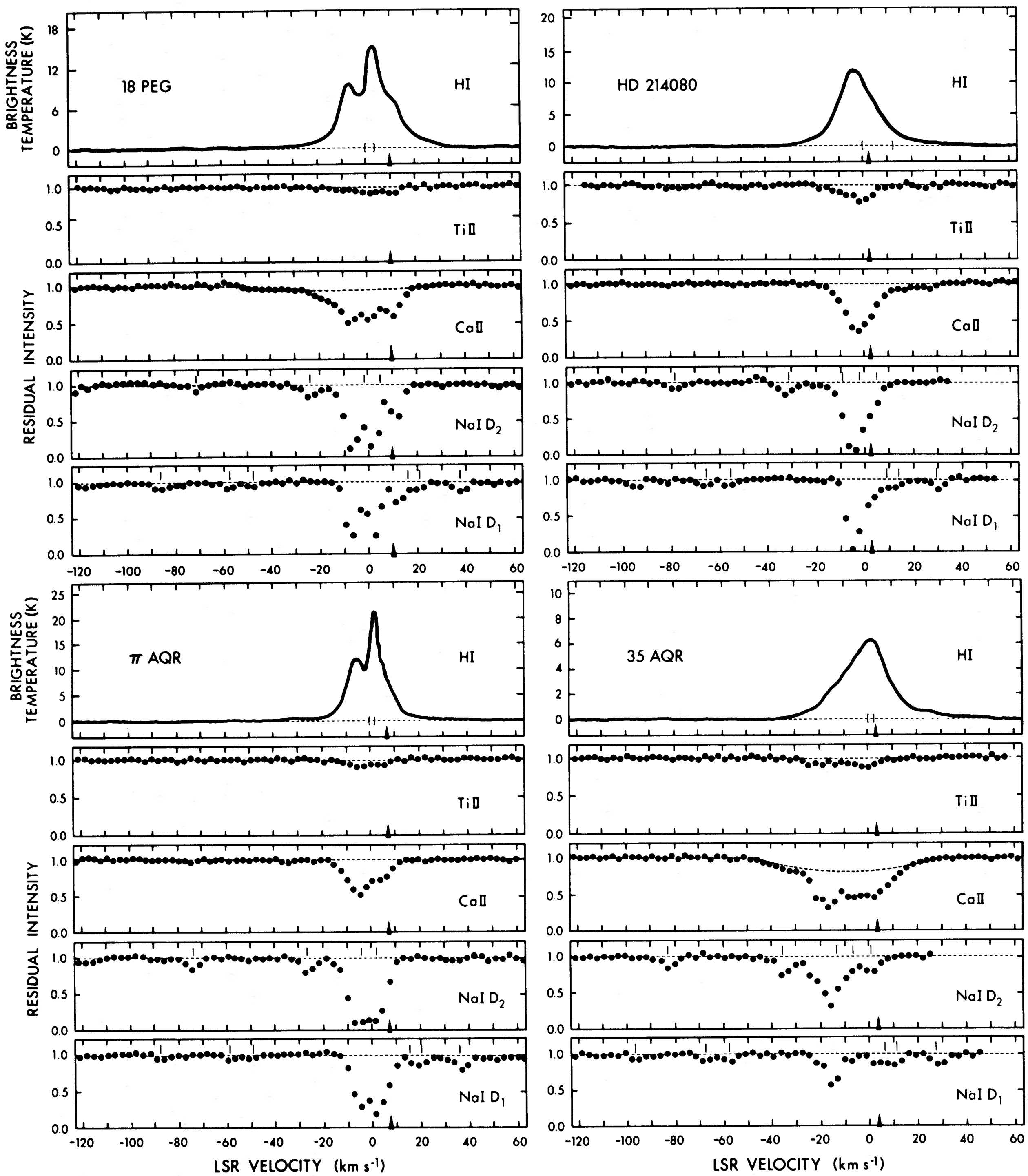

FIG. 2—*Continued*

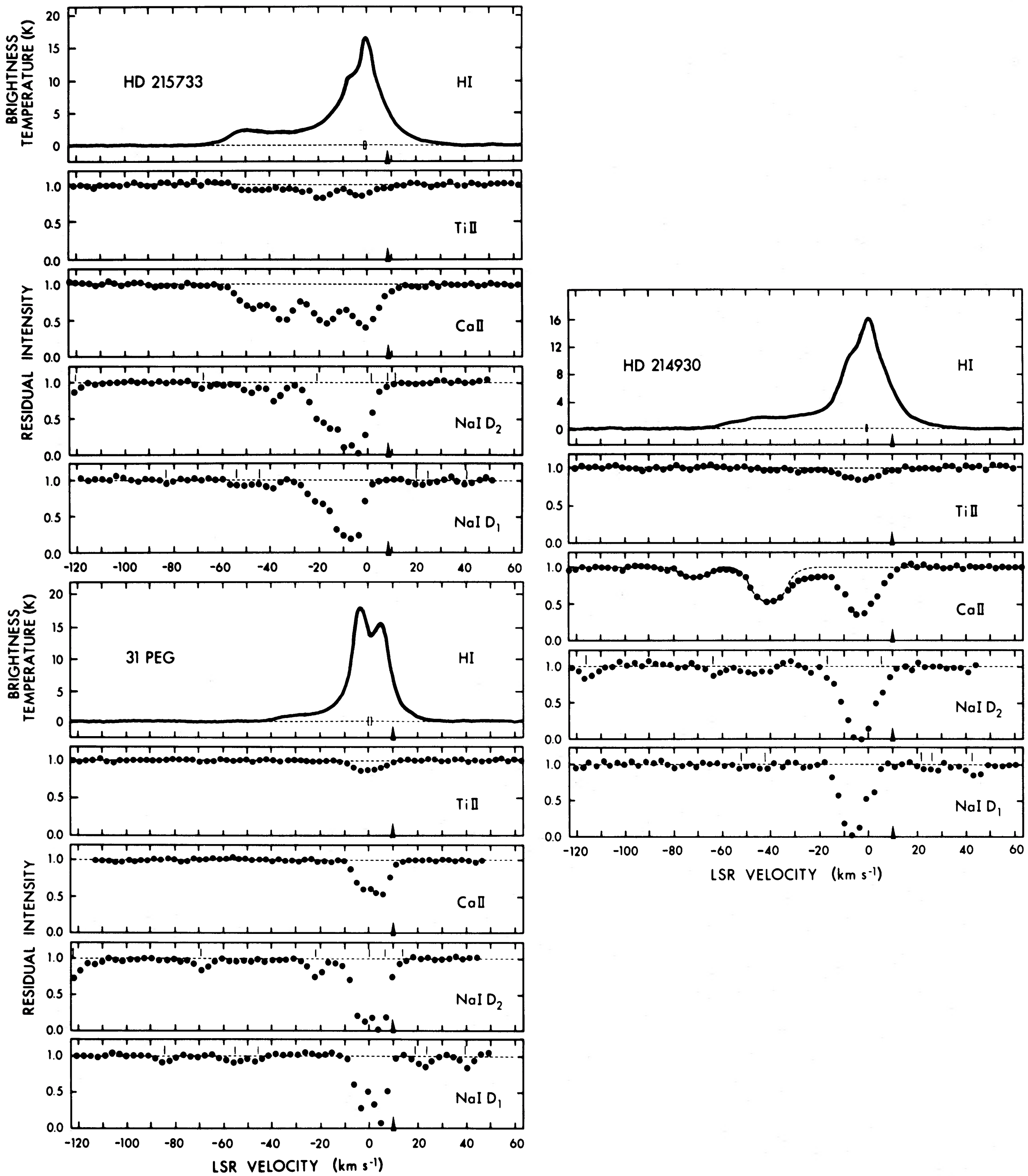

FIG. 2—*Continued*

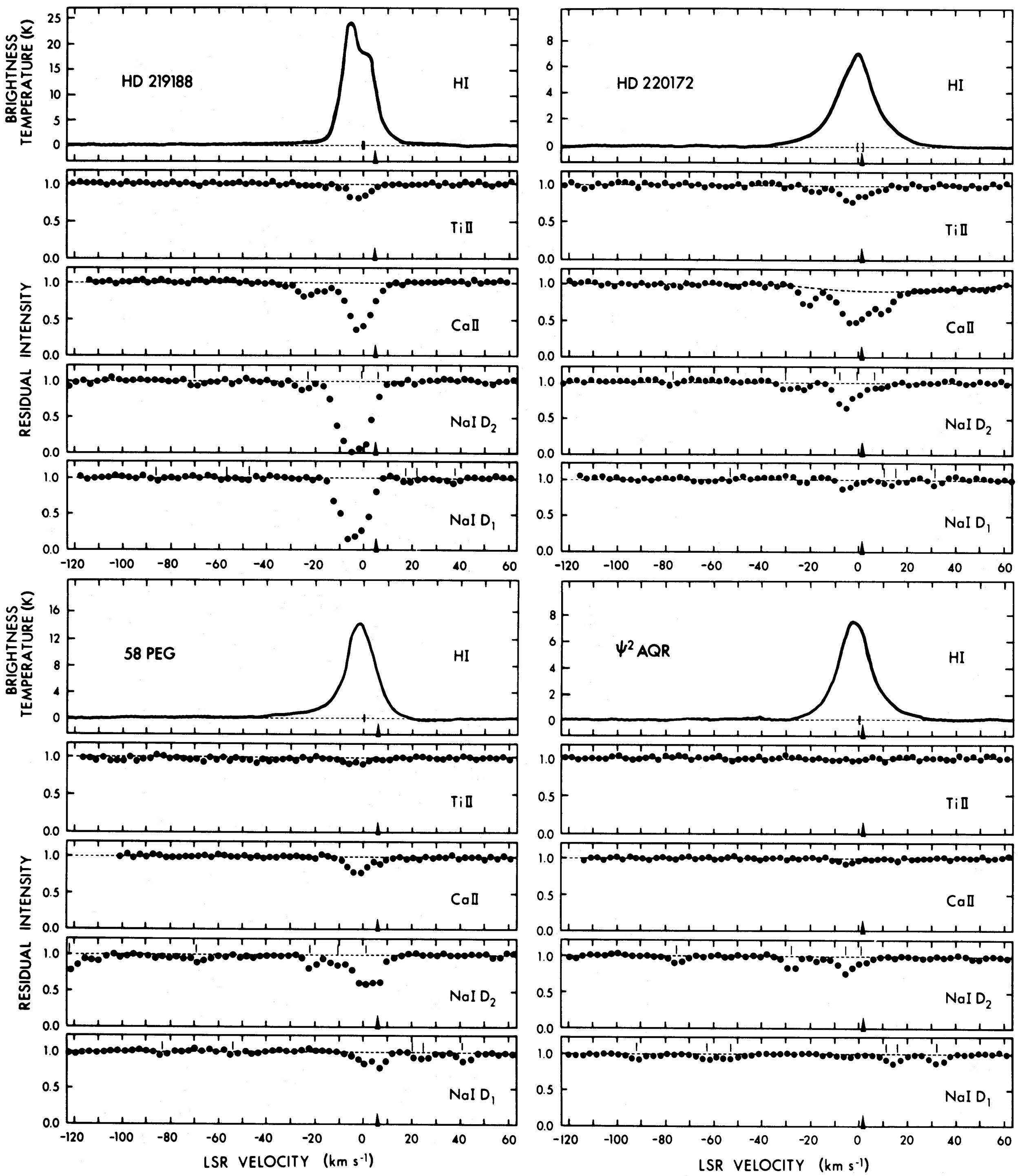

FIG. 2—*Continued*

TABLE 2

INTEGRATED EQUIVALENT WIDTHS AND COLUMN DENSITIES

	H I	Ti II		Ca II		Na I		
STAR	N(H I)[a] (10^{20} cm^{-2})	$W_\lambda(\lambda 3384)$ (mÅ)	N(Ti II) (10^{11} cm^{-2})	W_λ(K) (mÅ)	N(Ca II) (10^{11} cm^{-2})	$W_\lambda(D_2)$ (mÅ)	$W_\lambda(D_1)$ (mÅ)	N(Na I) (10^{11} cm^{-2})
HD 93521	1.7	37. ± 4.	12. ± 1.	202. ± 6.	26. ± 1.	...	135. ± 7.	19.–78.[b]
32 LMi	1.3	≤ 24.	≤ 7.2	≤ 12.	≤ 1.3	≤ 7.0	≤ 7.0	≤ 0.4
HD 97991	3.2	47. ± 9.	14. ± 3.	124. ± 16.	≥ 18.	135. ± 21.	151. ± 26.	22.–93.[b]
69 Leo	1.4	6.8 ± 3.8	2.1 ± 1.2	25. ± 5.	3.0 ± 0.5	55. ± 9.	32. ± 10.	3.4 ± 1.1
HD 119608	7.6	108. ± 20.	40. ± 7.	281. ± 24.	≥ 41.	278	202	> 30.[c]
85 Vir	4.6	≤ 17.	≤ 5.2	11. ± 6.	1.1 ± 0.6	87. ± 11.	52. ± 7.	5.6 ± 0.9
HD 149881	4.6	84. ± 13.	33. ± 5.2	252. ± 12.	> 41.	192. ± 19.	130. ± 15.	17.–59.[b]
HD 150483	1.2	6.5 ± 4.6	2.0 ± 1.4	9.8 ± 3.5	1.0 ± 0.4	10. ± 7.	5.6 ± 4.3	1.8 ± 1.4
18 Peg	5.0	22. ± 4.	6.8 ± 1.1	147. ± 6.	≥ 21.	294. ± 15.	228. ± 8.	> 39.
π Aqr	4.5	19. ± 3.	5.8 ± 0.9	96. ± 6.	13. ± 1.	280. ± 11.	232. ± 6.	> 33.
HD 214080	3.8	34. ± 6.	12. ± 2.	150. ± 7.	≥ 23.	207. ± 16.	171. ± 12.	> 46.
35 Aqr	2.6	34. ± 6.	11. ± 2.	285 ± 8.	29. ± 1.	164. ± 12.	90. ± 10.	> 11.
HD 215733	6.4	83. ± 14.	25. ± 4.	325. ± 6.	≥ 47.	356. ± 8.	278. ± 7.	41.[d]
HD 214930	5.7	44. ± 7.	13. ± 2.	184. ± 2.	≥ 27.	281. ± 13.	244. ± 11.	> 45.
31 Peg	4.7	22. ± 3.	7.3 ± 1.1	84. ± 4.	12. ± 1.	254. ± 16.	220. ± 11.	48.–52.[d]
HD 219188	5.6	25. ± 4.	8.1 ± 1.2	144. ± 7.	≥ 21.	296. ± 17.	235. ± 10.	> 41.
58 Peg	3.6	7.2 ± 6.1	2.2 ± 1.9	32. ± 8.	3.7 ± 0.9	89. ± 11.	53. ± 6.	5.5 ± 0.7
HD 220172	2.5	43. ± 7.	14. ± 2.	127. ± 8.	19. ± 2.	85. ± 12.	39. ± 7.	4.1 ± 0.7
ψ^2 Aqr	2.2	3.5 ± 1.8	0.8 ± 0.6	12. ± 4.	1.3 ± 0.4	...	5.2 ± 2.9	0.5 ± 0.3

[a] N(H I) calculated over the velocity interval of the Ca II K line components (see § II).

[b] N(Na I) lower limit determined from profile-fitting of the D lines (Table 3), while the upper limit includes at least one saturated component whose column density is an upper limit determined from the equivalent widths of the λ3302 doublet (Table 4).

[c] Equivalent widths from MZ; column densities derived from the doublet ratio method (Strömgren 1948; Nachman and Hobbs 1973).

[d] The integrated column density includes a saturated component whose lower limit from profile-fitting of the D lines (Table 3) is slightly greater than the upper limit from the λ3302 doublet (Table 4); the average column density is listed.

observed component equivalent widths in Table 3; however, in all cases, the total equivalent width was preserved. For essentially unsaturated lines, including all of the Ti II detections, the uncertainty in column density is scaled proportionally from that in the equivalent width. However, the K lines and particularly the D lines can be affected significantly by saturation, and the inferred column densities are correspondingly more uncertain. In such cases, the associated errors are represented by a letter code. Classification Y labels components whose central absorption is greater than 65% but less than 95% of the continuum intensity and whose column density uncertainties may range from 50% up to about a factor of 3. Classification Z denotes such strongly saturated lines that the central absorption is greater than 95%, so that only a lower limit can usefully be obtained on the corresponding column density. Five stars toward which the Na I D lines are strongly saturated were also observed at the generally unsaturated λ3302 doublet. Upper limits on the equivalent widths of the λ3302 lines are given in Table 4, providing rigorous upper limits to the Na I column densities along these lines of sight. The best fit line widths are also listed, in Table 3, for those components analyzed by the profile-fitting process, while for D line components with a doublet ratio in the range $1.3 \leq DR \leq 1.8$, the b-values can be estimated directly (Strömgren 1948) and are tabulated in the final column.

New observations of 21 cm emission lines of H I toward all of the stars were kindly obtained by Dr. Felix J. Lockman with the 140 foot (43 m) telescope of the National Radio Astronomy Observatory in 1981 June. The telescope has a half-power beam width of about 21′ at the H I frequency. The velocity resolution is 2.1 km s^{-1}, and the brightness temperatures were established by observations of the standard region S8 of Williams (1973). These spectra are also illustrated in

TABLE 3

COLUMN DENSITIES

		H I	Ti II				Ca II			Na I					
STAR	COMPONENT ($km\ s^{-1}$)	N(H I) (10^{20} cm^{-2})	W(λ3384) (mA)	N(Ti II) ($10^{11} cm^{-2}$)	b ($km\ s^{-1}$)	Ti/H (10^{-8})	W_λ(K) (mA)	N(Ca II) ($10^{11} cm^{-2}$)	b ($km\ s^{-1}$)	$W_\lambda(D_2)$ (mA)	$W_\lambda(D_1)$ (mA)	N(Na I)[a] ($10^{11} cm^{-2}$)	b($km\ s^{-1}$) D_1	D_2	DR
HD 93521	-58.3	0.18	10. ± 2.	3.2±0.6		≤1.75	29. ± 3.	3.5±0.3	6.6						
	-53.0	0.24	6.8± 1.4	2.1±0.4		0.86	26. ± 2.	3.1±0.3	4.7						
	-43.8	0.14	2.5± 1.4	0.8±0.4		0.55	9.9± 1.8	0.8±0.1	2.9						
	-35.4	0.11	≤1.6	≤0.5		≤0.44	12. ± 2.	1.6±0.3	3.3						
	-25.4	0.13	2.0± 1.3	0.6±0.4		0.47	7.2± 1.8	0.9±0.2	4.3		≤5.0	≤0.5			
	-15.0	0.23	8.3± 1.7	2.6±0.5		1.11	38. ± 2.	5.2±0.3	4.8		≤5.0	≤0.5			
	- 7.3	0.38	5.4± 1.5	1.7±0.5		0.44	53. ± 2.	7.5±0.2	4.0		104. ± 5.	>15.7 (Z)[b]		2.3	
	+ 4.4	0.12	2.3± 1.2	0.7±0.9		0.28	15. ± 2.	1.8±0.2	3.0		30. ± 5.	3.3± 0.6		3.3	
	+ 9.1	0.13					12. ± 2.	1.4±0.2	3.5		≤5.0	≤0.5			
32 LMi	- 9.3	0.55	≤16.	≤4.9		≤0.89	≤6.0	≤0.6		≤7.0	≤7.0	≤0.7			
	+ 3.4	0.08	≤7.6	≤2.3		≤2.91	≤6.3	≤0.7		≤7.0	≤7.0	≤0.7			
HD 97991	-19.5	0.70	9.8± 5.3	2.9±1.6	4.1	0.41	17. ± 8.	2.3±1.0	3.4	≤21.	≤21.	≤1.0	4.1	3.4	
	- 5.7	2.27	30. ± 6.	10.4±2.0	5.2	0.46	100. ±12.	15.0±1.8	5.4	135. ±21.	151. ±26.	21.7 (Y)			
	+ 4.7	0.25	6.8± 4.5	1.1±0.7	2.5	0.45	7.4± 6.0	0.7±0.6	1.5	≤21.	≤21.	≤1.0			
69 Leo	- 5.9	1.06	6.8± 3.8	2.1±1.2		0.20	21. ± 4.	2.4±0.4	2.8	55.± 9.	32. ±10.	3.4± 1.1	3.4	3.6	2.2
	+ 3.5	0.30	≤1.9	≤0.6		≤0.19	4.4± 2.3	0.6±0.3	2.1	≤8.3	≤8.3	≤0.4			
HD 119608	-33.2	0.09	≤9.4	≤2.9		≤3.20	11. ± 9.[c]	1.3±1.1	4.6						
	-23.2	0.15	9.3± 9.3	2.9±2.9		0.79	17. ± 7.	2.3±1.0	3.7						
	-16.8	0.21					14. ± 6.	2.3±0.9	0.7						
	- 8.9	2.46	18. ± 8.	6.5±3.0	4.6	0.26	44. ± 9.	6.1±1.2	5.0						
	+ 2.6	2.98	18. ± 5.	7.7±2.2	3.1	0.26	63. ± 9.	9.7±1.4	4.4	174	134	21.6 [d]			3.2
	+10.6	0.29	8.7± 6.8	3.5±2.7	4.3	1.19	14. ± 6.	2.0±0.9	1.7	104	68	8.3			2.7
	+19.2	1.01	39. ±11.	14.2±4.1	7.6	1.41	82. ±10.	13.3±1.6	5.7						
	+30.4	0.44	15. ± 8.	4.7±2.6	3.6	1.08	36. ±10.	3.9±1.1	4.0						
85 Vir	-16.2	0.36	≤17.	≤5.2		≤1.46	5.1± 4.2	0.5±0.4		≤6.6	≤6.6	≤0.3			
	- 7.5	3.15	≤17.	≤5.2		≤0.17	5.8± 4.2	0.6±0.5		74.± 9.	42. ± 5.	4.6± 0.6	4.8	3.1	3.5
	- 0.5	1.11	≤17.	≤5.2		≤0.47	≤4.3	≤0.5		13.± 6.	10. ± 5.	1.0± 0.7	3.8	0.5	0.2
HD 149881	-15.7	0.30	≤7.6	≤2.3		≤0.77	15. ± 4.	2.0±0.6	2.9	≤14.	≤11.	≤0.7			
	- 8.7	0.56	18. ± 7.	7.9±2.9	3.9	1.41	58. ± 5.	7.3±0.7	5.2	≤14.	≤11.	≤0.7			
	+ 1.1	2.22	39. ± 8.	16.6±3.4	5.9	0.75	96. ± 6.	19.1 (Y)	8.0	151. ±16.	113. ±13.	14.7 (Y)	4.4	4.3	2.9
	+ 8.5	1.37	27. ± 8.	8.3±2.5	4.3	0.60	73. ± 6.	11.1±0.9	6.4	40.8± 9.8	17. ± 8.	2.0± 0.7	2.8	4.9	
	+19.1	0.19	≤7.6	≤2.3		≤1.21	10. ± 5.	1.1±0.5		≤14.	≤11.	≤0.7			
HD 150483	- 9.0	0.76	6.5± 4.6	2.0±1.4		0.26	9.8± 3.5	1.0±0.4		10. ± 7.	5.6± 4.3	1.8± 1.4			
	+12.4	0.45	≤6.4	≤2.0		≤0.44	≤2.7	≤0.3		≤4.6	≤2.7	≤1.7			
18 Peg	-17.9	0.22	≤2.3	≤0.7		≤0.32	15. ± 3.	2.8±0.4	5.9	≤4.7	≤4.7	≤0.2			
	- 7.6	1.44	5.1± 2.3	1.6±0.7		0.11	55. ± 3.	7.0±0.4	4.5	123. ± 9.	104. ±5.	19.0 (Y)	2.7	2.2	
	+ 2.0	2.24	8.8± 2.1	2.7±0.6		0.12	41. ± 3.	7.8±0.5	5.2	119. ± 9.	89. ± 4.	16.3 (Y)	2.6	1.9	2.3
	+11.4	1.13	8.2± 2.0	2.5±0.6		0.22	36. ± 3.	3.8±0.4	3.1	52. ± 8.	35. ± 4.	3.9± 0.6	2.7	0.6	1.3

TABLE 3—*Continued*

STAR	COMPONENT ($km\ s^{-1}$)	H I: N(H I) (10^{20} cm^{-2})	Ti II: W(λ3384) (mA)	Ti II: N(Ti II) ($10^{11} cm^{-2}$)	Ti II: b ($km\ s^{-1}$)	Ti II: Ti/H (10^{-8})	Ca II: W_λ(K) (mA)	Ca II: N(Ca II) ($10^{11} cm^{-2}$)	Ca II: b ($km\ s^{-1}$)	Na I: $W_\lambda(D_2)$ (mA)	Na I: $W_\lambda(D_1)$ (mA)	Na I: N(Na I)[a] ($10^{11} cm^{-2}$)	Na I: b($km\ s^{-1}$) D_1	D_2	DR
π Aqr	− 4.8	3.26	13. ± 2.	3.9±0.7		0.12	73. ± 5.	9.8±0.7	5.8	157. ± 8.	118. ± 4.	24.1 (Y)	5.0	5.2	3.0
	+ 5.5	1.20	6.2± 1.8	1.9±0.6		0.16	23. ± 4.	2.7±0.4	3.2	123. ± 7.	114. ± 4.	9.0 (Y)	2.9	3.3	
HD 214080	− 9.3	0.67	9.3± 3.8	4.7±1.9	6.2	0.70	15. ± 3.	1.2±0.3	13.7	≤8.8	≤8.8	≤0.4			
	− 2.0	1.91	17. ± 4.	4.7±1.0	2.9	0.25	70. ± 3.	16.0±0.7	6.6	173. ±13.	149. ±10.	>41.3 (Z)	3.5	2.1	
	+ 3.5	0.70	7.1± 2.5	2.7±0.9	2.6	0.38	40. ± 3.	2.6±0.2	10.7	34. ± 9.	22. ± 6.	4.9± 2.1	2.7	8.1	1.0
	+10.4	0.32	≤4.0	≤1.2		≤0.38	10. ± 3.	1.1±0.3		≤8.8	≤8.8	≤0.4			
	+19.0	0.16	≤4.0	≤1.2		≤0.76	8.3± 3.1	0.9±0.3		≤8.8	≤8.8	≤0.4			
	+27.6	0.08	≤4.0	≤1.2		≤1.53	6.4± 3.1	0.7±0.3		≤8.8	≤8.8	≤0.4			
35 Aqr	−32.4	0.05	≤3.2	≤1.0		≤1.96	26. ± 4.	1.6±0.2	6.0	≤5.6	≤5.6	≤0.3			
	−21.5	0.16	9.9± 3.3	3.0±1.0		1.89	49. ± 3.	4.7±0.3	3.7	30. ± 6.	8.4± 4.0	1.3± 0.4	2.6	1.8	
	−14.7	0.42	6.7± 2.8	2.1±0.9		0.49	67. ± 3.	8.5±0.4	4.3	112. ± 7.	58. ± 6.	7.8 (Y)	3.5	2.5	
	− 7.5	0.46	5.5± 2.3	1.7±0.7		0.37	44. ± 3.	3.7±0.2	3.5	e	6.7± 4.0	0.4± 0.3	2.4	2.4	
	+ 1.8	1.23	12. ± 3.	3.8±1.0		0.31	73. ± 4.	9.8±0.5	6.6	22. ± 7.	17. ± 5.	1.7± 0.6	4.0	2.6	
	+11.9	0.31	≤3.2	≤1.0		≤0.32	26. ± 3.	1.0±0.1	5.5	≤5.6	≤5.6	≤0.3			
HD 215733	−49.7	0.48	6.3± 4.9	1.9±1.5		0.40	36. ± 2.	4.6±0.3	5.4	≤20.	≤20.	≤1.0			
	−43.9	0.28	7.9± 4.9	2.4±1.5		0.86	16. ± 2.	1.9±0.2	3.8						
	−34.1	0.46	8.8± 5.7	2.7±1.8		0.59	68. ± 2.	10.4±0.3	6.0	10. ± 3.	≤2.1	0.5± 0.1			
	−25.1	0.28	16. ± 4.	4.8±1.4		1.73	26. ± 2.	2.1±0.2	5.0	16. ± 3.	8.1± 3.1	0.8± 0.3			
	−17.4	0.84	19. ± 5.	5.7±1.6		0.68	63. ± 2.	11.3±0.4	5.8	90. ± 5.	59. ± 4.	6.7± 0.5	5.8	5.2	2.3
	− 8.3	1.13	5.9± 4.0	1.8±1.2		0.16	31. ± 2.	3.4±0.2	4.2	175. ± 4.	166. ± 4.	>30.4 (Z)	4.9	5.3	
	− 0.9	2.10	13. ± 5.	4.1±1.5		0.19	70. ± 2.	10.2±0.3	4.4	65. ± 3.	45. ± 3.	4.6± 0.3	3.7	2.0	1.5
	+ 5.8	0.80	5.7± 4.9	1.7±1.5		0.22	15. ± 2.	2.7±0.4	6.4	≤4.0	≤4.0	≤0.20			
HD 214930	−28.4	0.37	4.4± 3.4	1.4±1.0		0.36	25. ± 1.	2.7±0.2	7.8	≤7.9	≤7.9	≤0.4			
	−25.4	0.22	2.8± 2.7	0.9±0.8		0.39	13. ± 1.	1.4±0.1	8.1	≤7.9	≤7.9	≤0.4			
	−16.1	0.38	3.0± 2.6	0.9±0.8		0.24	13. ± 1.	1.6±0.1	3.9	≤7.9	≤7.9	≤0.4			
	− 5.9	1.89	16. ± 3.	4.8±1.0		0.25	75. ± 1.	13.0±0.2	5.2	233. ±11.	203. ± 9.	>41.0 (Z)	5.8	4.8	
	+ 0.1	2.04	12. ± 3.	3.6±0.8		0.18	39. ± 1.	5.7±0.1	3.9	48. ± 7.	41. ± 6.	4.1± 0.8	1.5	1.5	
	+ 5.8	0.79	5.6± 2.7	1.7±0.9		0.22	19. ± 1.	2.2±0.1	4.1						
31 Peg	− 4.0	2.02	8.9± 2.0	2.8±0.6	3.3	0.14	22. ± 2.	3.7±0.4	3.3	92. ±10.	78. ± 7.	13.2 (Y)	2.2	2.2	
	+ 0.3	1.02	8.3± 1.7	2.3±0.5	3.5	0.23	28. ± 2.	2.8±0.2	2.9	68. ± 7.	32. ± 4.	2.9± 0.4	1.2	1.2	
	+ 5.3	1.61	4.8± 1.7	2.2±0.8	3.6	0.14	34. ± 3.	5.4±0.4	2.7	94. ±10.	110. ± 7.	>31.8 (Z)	2.2	2.6	
HD 219188	−33.0	0.06	≤2.6	≤0.8		≤1.33	5.5± 3.3	0.6±0.4		≤6.6	≤6.6	≤0.3			
	−24.4	0.11	≤2.6	≤0.8		≤0.73	18. ± 3.	2.8±0.5	4.8	≤6.6	≤6.6	≤0.3			
	−16.1	0.26	≤2.6	≤0.8		≤0.31	14. ± 3.	1.3±0.3	3.6	≤6.6	≤6.6	≤0.3			
	− 2.8	4.20	18. ± 3.	6.8±1.1	4.8	0.16	84. ± 4.	13.5±0.6	5.3	239. ±14.	207. ± 9.	>35.6 (Z)	5.3	5.1	
	+ 2.9	1.00	6.6± 2.1	1.3±0.4	3.3	0.13	22. ± 3.	2.7±0.4	4.9	57. ±10.	28. ± 4.	5.3± 0.9	2.8	2.1	
58 Peg	− 9.7	0.22	≤4.4	≤1.4		≤0.64	≤5.6	≤0.6		9.6± 6.7	3.2± 2.8	0.4± 0.3			
	− 2.4	2.67	7.2± 6.1	2.2±1.9		0.08	26. ± 6.	3.2±0.8	4.5	33. ± 6.	17. ± 3.	2.4± 0.5		3.8	
	+ 6.0	0.73	≤4.4	≤1.4		≤0.19	6.0± 4.9	0.5±0.4	1.1	46. ± 7.	33. ± 4.	2.7± 0.4		3.4	1.0

1983ApJ...272..509A

TABLE 3—*Continued*

STAR	COMPONENT (km s^{-1})	H I: N(H I) (10^{20} cm^{-2})	Ti II: W(λ3384) (mA)	Ti II: N(Ti II) (10^{11}cm^{-2})	Ti II: b (km s^{-1})	Ti II: Ti/H (10^{-8})	Ca II: W_λ(K) (mA)	Ca II: N(Ca II) (10^{11}cm^{-2})	Ca II: b (km s^{-1})	Na I: $W_\lambda(D_2)$ (mA)	Na I: $W_\lambda(D_1)$ (mA)	Na I: N(Na I)[a] (10^{11}cm^{-2})	Na I: b(km s^{-1}) D_1	D_2	DR
HD 220172	-20.7	0.14	4.4± 2.6	1.4±0.8		0.96	8.9± 3.7	2.6±1.1	3.2	15. ± 6.	6.3± 3.3	0.7± 0.3			
	-14.0	0.15	4.9± 2.6	1.5±0.8		1.01	3.9± 3.0	0.3±0.3	3.2	≤4.5	≤4.5	≤0.2			
	- 8.4	0.46	5.9± 2.6	2.1±0.9	3.3	0.46	8.4± 3.0	1.4±0.5	2.2	≤4.5	≤4.5	≤0.2			
	- 1.4	1.21	19. ± 3.	7.0±1.2	4.0	0.58	53. ± 4.	8.4±0.6	4.3	43. ± 7.	19. ± 4.	2.0± 0.4			
	+ 4.6	0.15	8.3± 2.6	2.4±0.7	2.4	1.57	19. ± 3.	0.9±0.1	1.4	17. ± 5.	8.6± 3.3	0.9± 0.3			
	+11.0	0.35	≤3.7	≤1.1		≤0.31	34. ± 4.	5.0±0.5	5.2	10. ± 5.	4.6± 3.3	0.5± 0.3			
γ^2 Aqr	- 3.7	1.50	2.5± 1.8	0.8±0.6		0.05	8.3± 2.6	0.9±0.3		•	5.2± 2.9	0.5± 0.3			
	+ 5.2	0.56	≤2.0	≤0.6		≤0.11	1.8± 2.0	0.2±0.2		≤2.7	≤2.7	≤0.1			
	+14.9	0.12	≤2.0	≤0.6		≤0.50	2.2± 2.0	0.2±0.2		≤2.7	≤2.7	≤0.1			

[a] N(Na I) is taken as the average of $N(D_2)$ and $N(D_1)$.

[b] This interferometric scan of the D_1 line along the line of sight to HD 93521 was kindly provided by Hobbs 1978*a*, who obtained from the optical depth integrals a column density for the strongly saturated component of greater than 24×10^{11} cm^{-2}.

[c] A possible stellar K line (MZ) could be hidden in this rather noisy spectrum; a line of $v \sin i = 55$ km s^{-1} centered on the heliocentric radial velocity of +23 km s^{-1} would decrease the reported interstellar line strengths of the components at +2.6, +10.6, +19.2, and +30.4 km s^{-1} (LSR).

[d] Spectrum and equivalent widths from MZ; column densities derived from the doublet-ratio method (Strömgren 1948; Nachman and Hobbs 1973).

[e] D_2 lines severely contaminated with telluric contributions.

TABLE 4

INTERSTELLAR λ3302 LINES

Star	Component (km s^{-1})	$W_\lambda(U_2)$ (mÅ)	$W_\lambda(U_1)$ (mÅ)	N(Na I) (10^{11} cm^{-2})
HD 93521	−7.3	≤ 5.0	≤ 5.0	≤ 39.
	+4.4	≤ 5.0	...	≤ 39.
HD 97991	−5.7	≤ 12.	...	≤ 93.
HD 149881 ...	+1.1	≤ 7.4	...	≤ 57.
HD 215733 ...	−8.3	≤ 3.6	≤ 1.7	≤ 27.
31 Peg	+4.7	≤ 4.0	≤ 3.0	≤ 36.

Figure 2. The total column densities of neutral hydrogen along each line of sight are given in Table 2 and were calculated from the integrated brightness temperatures across the emission line, under the assumption that the emitting material is optically thin to 21 cm radiation. In general, even toward the background halo stars, the H I emission covers a slightly wider velocity range than the optical absorption (Fig. 2). However, to enable a direct comparison with the total column densities of the absorption lines, the total H I column density along each line of sight in Table 2 was computed only over the velocity range of the corresponding Ca II absorption. Alternatively, integrating the entire H I emission profile (to a signal level exceeding the root-mean-square fluctuation in each spectrum by a factor of 3) toward all the background halo stars results in less than a 15% increase in the total H I column densities over those obtained under the previous definition. Likewise, individual kinematic components were defined by the velocity limits of resolved features in the K lines, and the resulting component column densities are listed in Table 3.

The interpretation of the 21 cm H I emission observations requires three fundamental assumptions. First, the assumption that the H I source fills the 21′ beam seems generally plausible, since the 21 cm profiles toward the nine foreground and background star pairs, separated by up to several degrees, show generally good agreement. The velocities of the strong optical lines also show good agreement in all but one case; that one case, the pair HD 214080 and 35 Aqr, with an angular separation of 6°.7, will not be considered as a foreground-background pair in the following discussions. Further, Habing (1969) has mapped the 21 cm emission surrounding three of the program stars and finds that the features typically extend over areas of several square degrees. Of course, this does not preclude some small-scale patchiness in the distribution of the individual absorbing clouds, which is probably reflected in the scatter of their properties when analyzed on a component by component basis. Second, the assumption that no significant systematic corrections are required to these data for stray radiation possibly received in the 140′ telescope sidelobes needs some justification. The importance of such stray radiation in artificially raising the observed column density of neutral hydrogen can be estimated by comparing the 21 cm emission column density with that obtained from Lyα absorption observations. Five of the six stars with $|z| \geq 1.5$ kpc of this study have column densities determined by these two techniques that are identical to within their errors (HMAL), directly suggesting that stray radiation in the radio measurements is negligible within the observational uncertainties. Finally, it is assumed that the H I column density is an adequate approximation to the total amount of hydrogen along these high-latitude lines of sight. Five of the present program stars were included in the survey of interstellar molecular hydrogen carried out by Savage *et al.* (1977); with the exception of material toward HD 219188, for which 6% of the hydrogen is in molecular form, the amount of H_2 along these lines of sight is very small. From measurements toward seven high-latitude stars, Savage *et al.* conclude that there is no evidence for the existence of appreciable amounts of H_2 in the halo gas.

III. LINE STRENGTHS AND VELOCITIES

The primary purpose of this study is to compare, at high detection sensitivity and high velocity resolution, both the optical heavy-element absorption and the corresponding 21 cm emission seen toward distant halo stars with that seen toward nearly aligned, high-latitude foreground stars in the disk. It must be emphasized, however, that the regions of the disk and halo so studied are arbitrarily set by the distances of the stars included in the sample. In particular, "the disk" observed here is *defined* as that part of each path length toward the foreground star, which (excluding 35 Aqr as previously discussed) ranges in z-distance from 50 to 230 pc with an average of 120 pc. "The halo" is then *defined* as the remaining path length beyond each foreground star to the more distant high-z star, at an average z-distance of 1.5 kpc. The detailed comparison of "disk" and "halo" gas observed toward each pair of foreground and background stars is then constrained by their angular separations, as listed in Table 1. Although both the 21 cm emission profiles and the velocities of the optical absorption lines show generally good agreement (Fig. 2), the linear separation of 13 pc in Table 1 slightly exceeds the 10 pc diameter of Spitzer's (1978) standard diffuse cloud; hence, even the local portions of each line of sight could be somewhat different.

The interpretation of these observations as representative of interstellar material in the lower galactic halo includes the implicit assumption that the spectra are not contaminated appreciably by gas that may still be associated with the recently formed background OB stars. This assumption is most strongly supported by Figure 3, which demonstrates that there is not a significant correlation between the radial velocities of each halo star and those of the clouds observed along its line of sight. In addition, since Ti II is a dominant ionization stage in H I regions, the strong Ti II absorption detected toward the halo stars of this study and the coincidence of the individual kinematic components of Ti II and Ca II indicate that the observed halo clouds are almost certainly not H II regions. Absorption is also detected toward two of the foreground stars of spectral type A, which would not be expected to form extensive H II regions. Further, although absorption lines could, in principle, be produced in dense neutral shells surrounding H II regions, such shells are unlikely toward these unreddened stars, and a plot of line strength with stellar distance, comparable to Figure 4, shows the generally smooth increase expected for absorption formed in a diffuse medium. Similar evidence led Stokes (1978) to conclude that a large majority of the Ti II gas observed in his extensive survey of the galactic disk likewise did not appear to be associated with either circumstellar H II regions or their neutral shells.

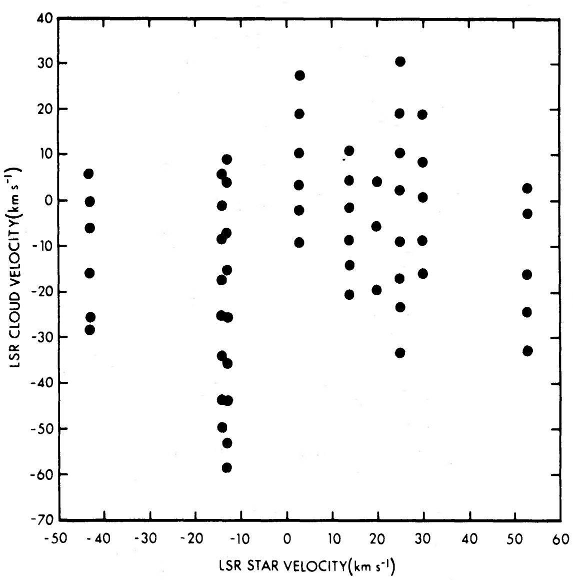

FIG. 3.—Correlation between LSR radial velocities of background halo ($|z| > 500$ pc) stars and velocities of interstellar clouds observed along each line of sight.

The interstellar material observed, as described above, in the two regions of high-latitude disk and halo can be compared in terms of the absorption-line strengths, the velocity ranges of the absorption, and the elemental abundance ratios. The last considerations are deferred to § IV. Although the stars surveyed are equally distributed between positive and negative galactic latitudes, the total number of observed lines of sight is not sufficient to permit comparison of the different hemispheres; therefore, for simplicity in the following discussions, "the absolute value of z" is replaced by "z".

a) *Line Strengths*

The directly observed Ti II, Ca II, and Na I equivalent widths are illustrated as bar graphs in Figure 4. The thickness of each bar is proportional to the total integrated equivalent width observed within the indicated velocity ranges toward the 19 high-latitude stars of the present study. Absorption by all three ions along all lines of sight increases from the foreground disk to the background halo star. Excepting only the HD 215733 line of sight, where the Na I seems to be almost entirely below the foreground star, and HD 220172, where the Na I lines are unsaturated, the D line is relatively weak toward the foreground absorption (Fig. 4*c*) star and saturated toward the halo star. Hobbs (1971) has compared the sodium D lines and H I 21 cm line toward 30 stars at intermediate and high galactic latitudes whose distances are similar to those of the foreground high-latitude disk stars studied here. He found that 64% of the lines observed had a value $Q \equiv N(\text{Na I})/N(\text{H I})$ within a factor of 2 of an average value of about 4×10^{-9}. It is not surprising that the 21 cm emission column densities toward all the stars of this study are comparable to those of Hobbs, and that the Q-values for the foreground stars also average 4×10^{-9}; however, $\langle Q \rangle = 13 \times 10^{-9}$ for the high-z stars, confirming that a substantial amount of optically absorbing gas exists above the foreground disk stars.

Strong Ca II absorption has been frequently observed toward halo sources (MZ; Greenstein 1968; Cohen 1974; Cohen and Meloy 1975), and Figure 4*b* demonstrates the dramatic increase of the K line strength with increasing distance above the galactic plane. The line strengths attained toward the high-z stars here are similar to those observed in the disk along path lengths of about 1–2 kpc.

The great strength of the Ti II absorption perpendicular to the plane of the Galaxy (Fig. 4a) was reported and discussed in Paper I. Toward the foreground disk stars, the Ti II line strengths are comparable to those observed in Stokes's (1978) high-resolution photoelectric survey of 68 stars in the solar neighborhood, whereas lines of the strength observed toward the halo stars would be

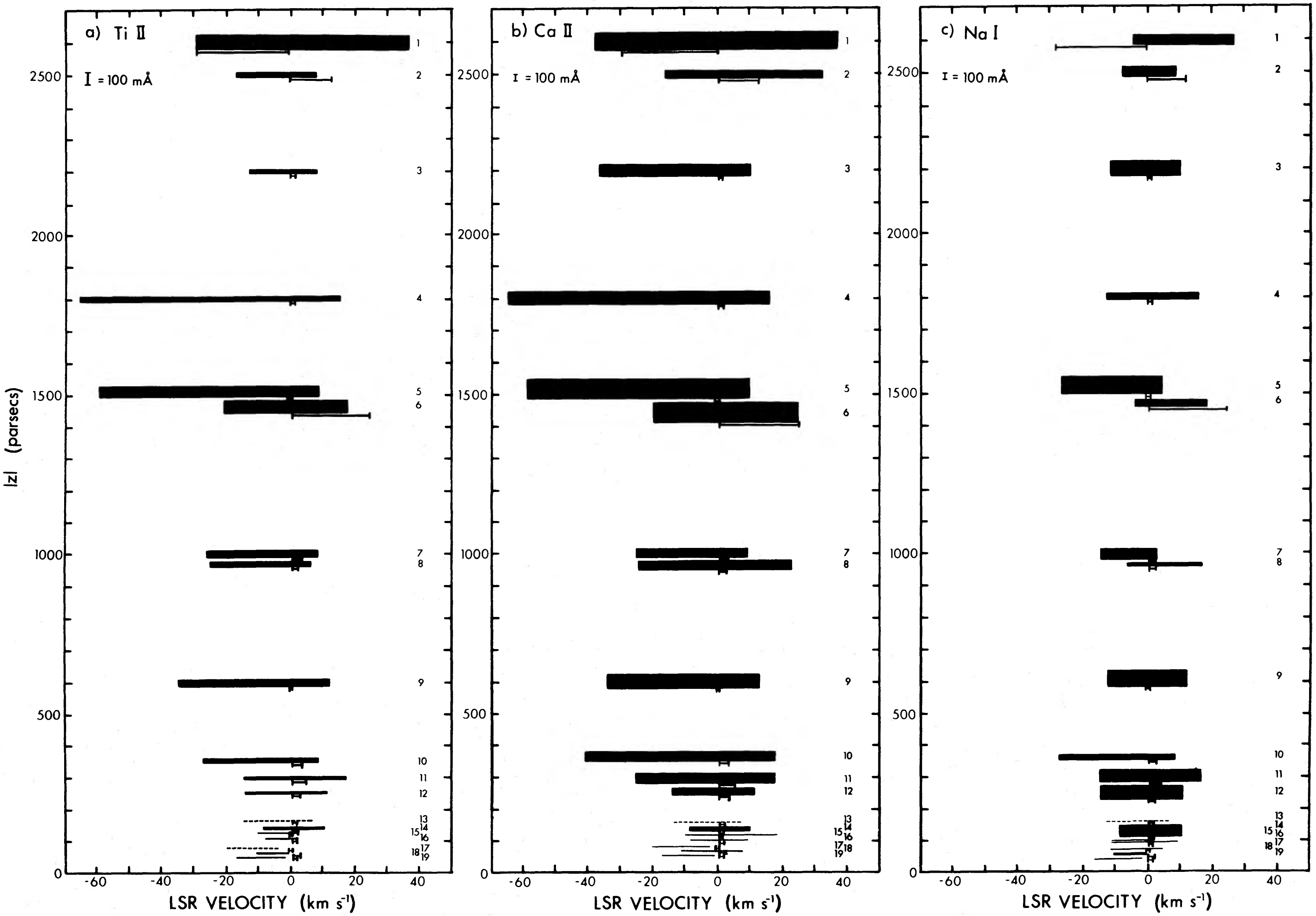

FIG. 4.—Integrated Ti II (a), Ca II (b), and Na I (c) equivalent widths toward 19 high-latitude stars. The vertical height of each bar is proportional to the total observed equivalent width within the indicated velocity ranges. The small symbol in the upper left-hand corner denotes the height corresponding to an equivalent width of 100 mÅ. The thin lines under each bar mark the velocity range predicted for corotating material along the line of sight toward each star. The stars are: (1) HD 119608, (2) HD 214080, (3) HD 219188, (4) HD 93521, (5) HD 215733, (6) HD 149881, (7) HD 97991, (8) HD 220172, (9) HD 214930, (10) 35 Aqr, (11) 18 Peg, (12) π Aqr, (13) 32 LMi, (14) 31 Peg, (15) ψ^2 Aqr, (16) 58 Peg, (17) 85 Vir, (18) 69 Leo, (19) HD 150483.

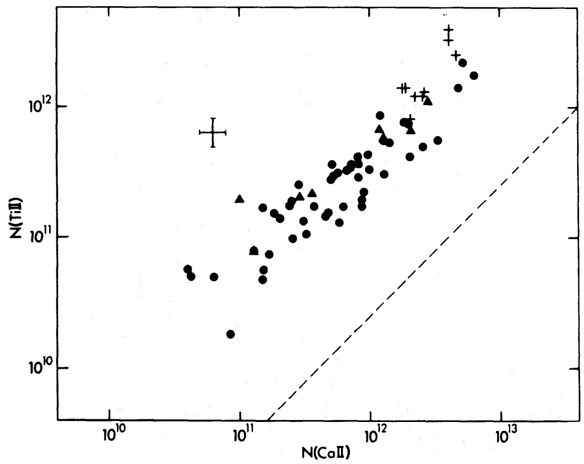

FIG. 5.—The correlation diagram for integrated column densities of Ti II and Ca II toward 48 stars in the disk (Stokes 1978) and 19 high-latitude stars. Disk stars are represented by circles, while high-latitude stars with $|z| > 500$ pc and $|z| \leq 360$ pc are denoted by crosses and triangles, respectively. The dashed line indicates the relationship that would be expected if both Ca II and Ti II were dominant ionization states and were present in their cosmic abundance ratio, $A_{\rm Ca}/A_{\rm Ti} = 39$ (Withbroe 1971). Typical observational uncertainties are illustrated by the vertical and horizontal bars in the upper left corner.

expected to arise in typical disk material over extrapolated path lengths of about 3 kpc. Thus, interstellar gas in the halo produces strong absorption in all three of the heavy ions observed in the present study. Stokes demonstrated that, in contrast to the strong variations of the titanium abundance relative to sodium, potassium, and the grains responsible for interstellar reddening, the ratio of column densities of titanium and calcium remains relatively constant in the disk at about 4 times the solar value. Figure 5 reproduces his correlation diagram for these two ions and shows that the strong correlation is preserved above the galactic plane. As in the plane, Na I therefore appears to be nearly undepleted, while Ca II and Ti II individually vary widely in gas phase abundance but maintain a relatively constant ratio of depletions (§ IV).

A more quantitative comparison of the absorption produced along the line of sight toward each high-z star with that toward its corresponding foreground star is provided by calculating the fraction of the column density along each line of sight that arises in the halo: $(N_{\rm total} - N_{\rm disk})/N_{\rm total}$, where $N_{\rm total}$ is the column density observed toward the background halo star, and $N_{\rm disk}$ is that observed toward the nearly aligned foreground disk star. Table 5 lists the fractions of Ti II, Ca II, and Na I column densities produced in the halo along every line of sight, including the halo path length between HD 214930 and HD 215733. Ranges are quoted for those lines of sight where only an upper limit to the absorption toward the foreground star is observed. With the exception of 18 Peg and its foreground star at roughly similar z-distances of, respectively, 300 and 230 pc, approximately 50%–95% of the column densities of all three ions are produced by material above the foreground stars. If the optically absorbing gas extends well beyond the foreground disk stars, the fraction of the absorption arising in the halo should increase with increasing halo path length. Figure 6 plots the fraction of halo absorption along each line of sight as a function of the ratio of the z-distances of the halo and foreground stars, $z_{\rm halo}/z_{\rm disk}$. For all three ions, this fraction behaves similarly, rising from a value necessarily approaching zero as $z_{\rm halo}/z_{\rm disk}$ approaches unity, but increasing with increasing halo path length until $z_{\rm halo}/z_{\rm disk}$ lies in the range 4.0–7.5. Beyond this turning point, which can be crudely represented, for the average $z_{\rm disk}$ of 120 pc, by a characteristic height $z_{\rm halo}$ on the order of 500–900 pc, the halo contribution to each line of sight remains

TABLE 5

FRACTION OF ABSORPTION ARISING IN THE HALO[a] ALONG EACH LINE OF SIGHT

Line of Sight	Ti II	Ca II	Na I
HD 93521/32 LMi	0.40–1.00	0.96–1.00	0.98–0.99
HD 97991/69 Leo	0.86	0.83	0.85–0.92
HD 119608/85 Vir	0.87–1.00	0.98	> 0.81
HD 149881/150483 ...	0.94	0.98	0.89–0.93
18 Peg/π Aqr	0.15	0.38	0.15
HD 215733/214930 ...	0.48	0.43	0[b]
HD 215733/31 Peg ...	0.72	0.74	0[b]
HD 214930/31 Peg ...	0.46	0.56	0[b]
HD 219188/58 Peg ...	0.73	0.81	> 0.87
HD 220172/ψ^2 Aqr ...	0.94	0.93	0.88

[a]As defined in the text (§ III).

[b]$N_{\rm disk} > N_{\rm total}$; essentially all Na I along this line of sight is below 31 Peg.

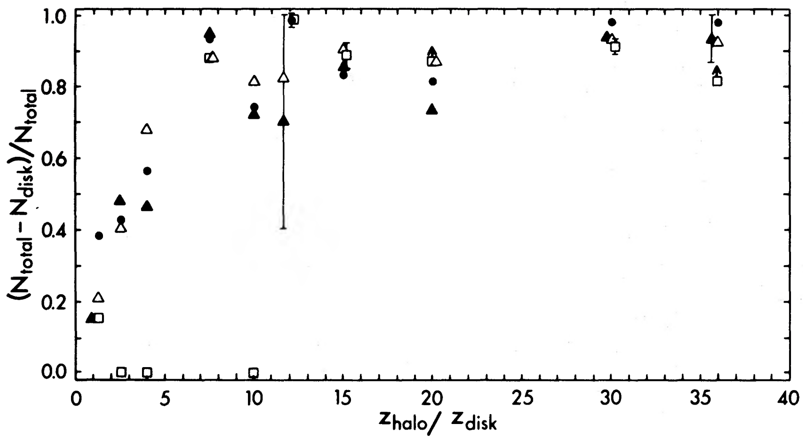

FIG. 6.—The fraction of absorption arising in the halo along each line of sight as a function of the ratio of the z-distances of the halo and foreground stars. Ti II, Ca II, and Na I absorptions are denoted by filled triangles, circles, and squares, respectively. Bars indicate absorption ranges along those lines of sight for which only upper limits were obtained toward the foreground star. The corresponding fraction of H I along the halo portion of each line of sight cannot be observed directly, since H I absorption measurements are likely to remain generally unavailable toward the foreground stars of later spectral type; however, this fraction can be predicted from a model exponential gas distribution with a scale height of 900 pc (§ IVb) and is represented by open triangles.

constant at approximately 85%–90%. If the gas were confined to a thin disk below the foreground stars, this halo fraction would remain at zero. If the gaseous disk were somewhat extended but its density decreased rapidly beyond the foreground stars, this fraction would remain relatively low. Instead, along seven of the lines of sight, the Ti II, Ca II, and Na I absorption lines observed toward the high-z star are indeed formed almost completely in the halo.

Thus, there is evidently a very slow decrease in the gaseous density of all three ions above the galactic plane, strengthening the same conclusion reached in Paper I for Ti II alone. In particular, these observations demonstrate that the optically absorbing gaseous layer of our Galaxy is much thicker than both the traditionally quoted scale heights of 50–60 pc for OB stars and of 120 pc for the interstellar gas and dust (Mihalas and Binney 1981). Quantitative models of the vertical distribution of the gas are developed in § IV.

b) *Velocity Ranges of the Absorption*

The directly observed equivalent widths, illustrated as bar graphs in Figure 4, clearly show that not only do all line strengths increase above the foreground disk stars, but also the velocity ranges of the Ti II and Ca II absorption increase markedly with distance above the galactic plane. This confirms the original conclusion of MZ for Ca II absorption, now generalized to include the similar behavior of Ti II, which, in contrast to Ca II, requires no uncertain corrections for other stages of ionization. Figure 7 plots the fraction of absorption arising in the halo for all three ions, calculated as in Table 5 and Figure 6, but now determined for each individual kinematic component as a function of its velocity. A significant amount of disk gas, defined as that seen in absorption against the foreground stars, is observed in all three ions and is exclusively at low velocity, within ± 10 km s^{-1} of zero velocity in the LSR frame. In contrast, halo gas beyond the foreground disk stars is observed at both low and high velocities. The low-velocity gas in the halo includes a substantial fraction of the total low-velocity gas observed in all three ions. One of the primary results of this study is that gas at velocities $|v| > 10$ km s^{-1}, however, is observed only above the foreground stars and only in the lines of Ca II and Ti II, with the important exception of four Na I components, three of which are along the line of sight toward the one star HD 215733. The spectra themselves (Fig. 2) show excellent correlation between the velocities of the various components of Ca II and Ti II, implying that both the low- and high-velocity gas are dominantly cool and neutral.

The total H I column density corresponding to the optically absorbing halo gas at $|v| > 10$ km s^{-1} can be calculated from the 21 cm emission as given in Table 3; another of the primary results of this study is that this gas constitutes 24% of the entire H I column density over all velocities toward the high-z stars. Since the total column density derived from 21 cm emission includes contributions from material in the disk, this also sets a rigorous lower limit of one-fourth on the amount of high-velocity ($|v| > 10$ km s^{-1}) halo gas relative to the total observed halo gas.

It would be of great interest to compare the amount and distribution of the observed cold gas with that of warm halo gas. From observations of halo gas in the ultraviolet absorption lines of Si II and Si IV seen along the line of sight to the Large Magellanic Cloud, Savage

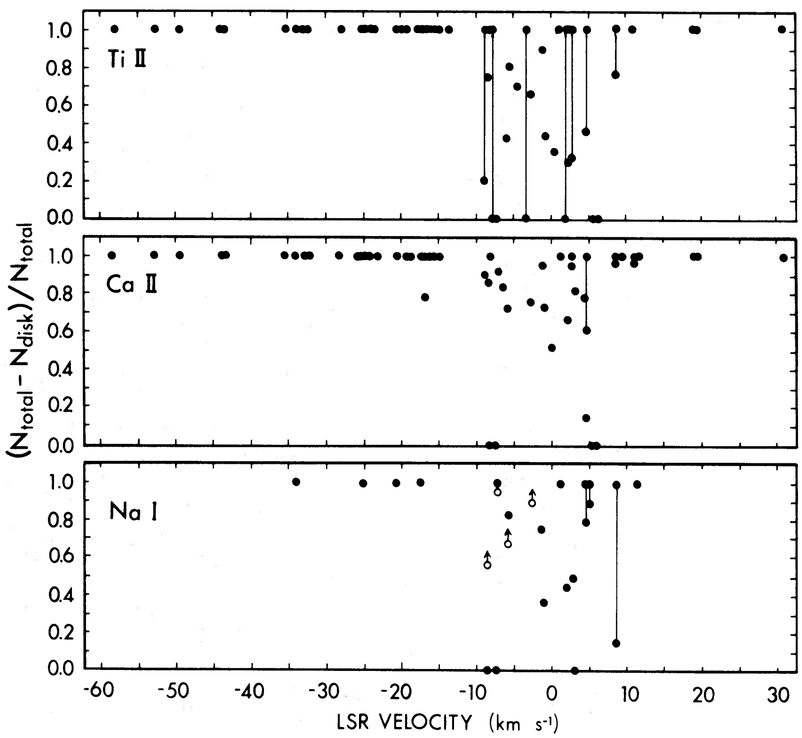

FIG. 7.—The fraction of Ti II, Ca II, and Na I absorption arising in the halo for each individual kinematic component from Table 3. Bars indicate absorption ranges along those lines of sight for which only upper limits were obtained toward the foreground star. Open circles denote saturated components.

and de Boer (1981) estimated that the mass of cold halo gas exceeds that of the warm gas by a factor of 10. However, the lower resolution *International Ultraviolet Explorer* (*IUE*) observations necessitated a kinematic definition of halo gas as that with $|v_{LSR}| > 25$ km s^{-1}, and they cannot be compared directly with the current high-resolution study.

The present observations of the strengths and velocity ranges of optical absorption lines suggest a simple picture of the cool, neutral interstellar material in the lower halo. There are two distinct types of gas above the galactic plane: a thick low-velocity disk (type A) extending well beyond the 120 pc average z-distance of the foreground stars, which produces strong absorption lines of Na I, Ca II, and Ti II, and additional gas (type B) at high velocity observed only at large z-distances which contains more than 24% of the mass of the observed cool halo gas and which produces strong absorption lines of Ca II and Ti II but not of Na I. The implications of this picture will be further discussed in § V.

IV. THE ELEMENTAL ABUNDANCES

a) *The Observed Titanium Abundances*

Since the λ3384 line remains generally optically thin, and since Ti II is the dominant ionization stage of titanium in H I regions, the λ3384 observations provide a unique opportunity, within the statistical limitations of the observations, to model the depletion of the interstellar gas with height above the galactic plane.

The relation between the total integrated column densities of Ti II and H I given in Table 2 for each line of sight was discussed in Paper I. These observations show directly that, compared with well-studied disk abundances, interstellar gas in the lower halo is apparently characterized by decreased titanium depletion, i.e., increased gaseous titanium abundance. It is important to emphasize that the observed ratio N(Ti II)/N(H I) is a lower limit to the actual gaseous titanium abundance along the line of sight to the star, since the 21 cm emission lines also include contributions from neutral hydrogen beyond the target star. This effect is significant in practice only for the lower z stars of this study since, as previously discussed, HMAL demonstrated that there are not significant amounts of hydrogen beyond five of the six stars with $|z| \geq 1.5$ kpc. For the foreground stars, crude corrections to the observed lower limits on the titanium abundances can be obtained from a model of the H I present below the star. This corrected N(H I) can be estimated by subtracting from the total column density observed toward the corresponding halo star an assumed exponential halo gas distribution which

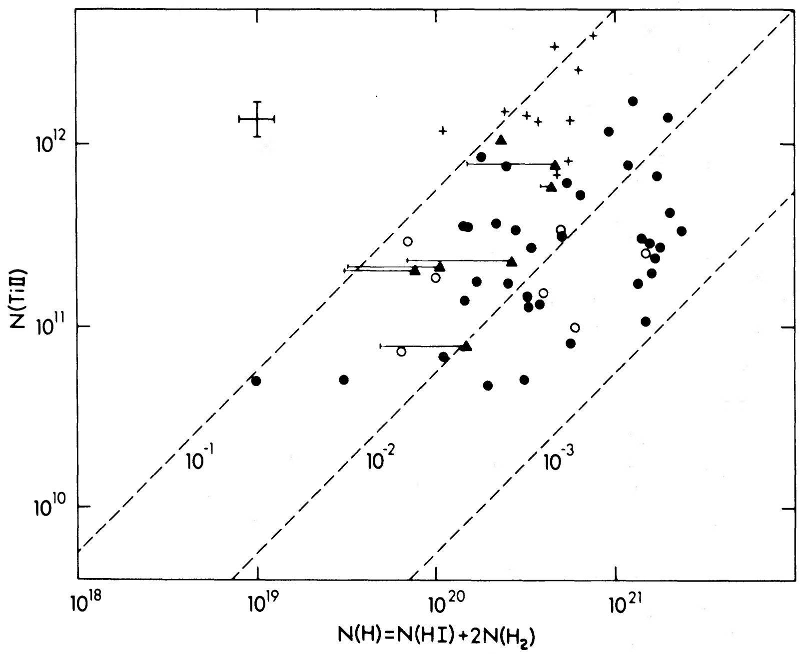

FIG. 8.—Integrated titanium column densities toward 43 disk stars (Stokes 1978) and 19 high-latitude stars. Disk stars are denoted by circles, with open circles indicating lines of sight for which corrections for molecular hydrogen are unavailable. High-latitude stars with $|z| > 500$ pc are denoted by crosses. High-latitude stars with $|z| \leq 360$ pc are represented by triangles and lines, as discussed in the text (§ IVa). The dashed diagonal lines indicate depletions of titanium δ_{Ti} of 10^{-1}, 10^{-2}, and 10^{-3}. Typical observational uncertainties are illustrated by the vertical and horizontal bars in the upper left corner.

is discussed in the following section. The results are shown in Figure 8, which reproduces the relation between N(Ti II) and N(H I) from Paper I, for Stokes's disk survey and for the present high-latitude sample. However, each foreground star is now represented by a line whose right-hand endpoint is the observed H I column density along the entire line of sight and whose left-hand endpoint represents the model-dependent estimate of the column density of H I actually below the foreground star. Although this plot represents lower limits to the titanium abundance, the limitations inherent in the H I emission observations serve to underestimate, rather than overestimate, the observed increase in gaseous titanium abundance above the plane. As concluded in Paper I, the high-latitude lines of sight are characterized by significantly lower depletion than the disk mean.

The depletions illustrated in Figure 8 are mean values, since the column densities are those integrated over all velocity components along each line of sight. The titanium depletions for separate kinematic components are defined as the ratio of the observed column densities of titanium relative to hydrogen to that ratio in the Sun, $\delta_{\mathrm{Ti}} \approx [N(\mathrm{Ti\ II})/N(\mathrm{H\ I})]/A_{\mathrm{Ti}}$, with $A_{\mathrm{Ti}} = 5.5 \times 10^{-8}$ (Withbroe 1971). These normalized abundances, whose reciprocals are the usual "depletion factors" (≥ 1), are listed in Table 6. In all cases, the individual cloud abundances are greater than Stokes's disk mean of 0.01; i.e., the gas phase abundances are greater than the 1% of the presumed total interstellar abundance typical of the disk. The largest of these abundances approach the solar value to within a factor of about 3. Table 6 also shows the correlation of depletion with velocity, previously noted in Paper I. The titanium gas phase abundances average $\langle \delta \rangle = 0.15$ for the 24 line components with $|v| > 10$ km s^{-1}, in contrast to an average of 0.06 for the 37 components with $|v| \leq 10$ km s^{-1}, so that the mean gas phase abundance of 0.10 could be formally produced by a mixture consisting of 44% by mass of the high-velocity, high-abundance type gas.

Thus, the gas phase abundance of titanium increases strongly above the plane of the Galaxy, with respect to the disk mean, and further increases with LSR velocity of the individual cloud components.

b) *Analytic Models of the Depletion and the Density above the Plane*

The observed ratio of the column densities can be expressed as

$$\frac{N_{\mathrm{Ti\,II}}}{N_{\mathrm{H\,I}}}(z) = \frac{\int_0^z \varphi(z)\, n_{\mathrm{H}}(z)\, dz}{\int_0^\infty n_{\mathrm{H}}(z)\, dz}, \tag{2}$$

TABLE 6

DEPLETIONS, INDIVIDUAL KINEMATIC COMPONENTS

STAR	Ti II DETECTION LIMIT $N(\mathrm{Ti\ II})\times10^{-11}$ cm^{-2}	LSR VELOCITY INTERVALS (km s^{-1}) −65 to −55	−55 to −45	−45 to −35	−35 to −25	−25 to −15	−15 to −5	−5 to +5	+5 to +15	+15 to +25	+25 to +35
$\lvert z\rvert > 500$ pc											
HD 93521	1.4	0.32	0.16	0.10, ≤ 0.08	0.09	0.20	0.08	0.05	...	...	...
HD 97991	1.6	...	...	...	...	0.07	0.08	0.08	...	...	...
HD 119608	2.9	...	...	...	≤ 0.58	0.14	0.05	0.05	0.22	0.26	0.20
HD 149881	2.3	...	...	...	...	≤ 0.14	0.26	0.14	0.11	≤ 0.22	...
HD 214080	1.2	...	...	...	...	...	0.13	0.05,0.07	≤ 0.07	≤ 0.14	≤ 0.28
HD 214930	1.0	...	...	...	0.07,0.07	0.04	0.05	0.03	0.04	...	...
HD 215733	1.7	...	0.07	0.16	0.11	0.31,0.12	0.03	0.04	0.04	...	...
HD 219188	0.8	...	...	...	≤ 0.24	≤ 0.13, ≤ 0.06	...	0.03,0.02	...	...	...
HD 220172	1.1	...	...	...	...	0.17	0.18,0.08	0.11,0.29	≤ 0.06	≤ 0.29	...
$\lvert z\rvert \le 360$ pc											
32 LMi	2.3	...	...	...	...	...	≤ 0.16	≤ 0.53	...	...	...
69 Leo	1.6	...	...	...	...	...	0.04	≤ 0.03	...	...	...
85 Vir	5.2	...	...	...	...	≤ 0.27	≤ 0.03	≤ 0.09	...	...	...
HD 150483	2.0	...	...	...	...	...	0.05	...	≤ 0.08	...	...
18 Peg	0.7	...	...	...	...	...	0.02	0.02	0.04	...	...
π Aqr	0.6	...	...	...	...	...	...	0.02,0.03	...	...	...
35 Aqr	1.0	...	...	...	≤ 0.36	0.34	0.09,0.07	0.06	0.06	...	...
31 Peg	0.7	...	...	...	...	...	...	0.03,0.04	0.03	...	...
58 Peg	1.4	...	...	...	...	...	≤ 0.12	0.01	0.03	...	...
ψ^2 Aqr	0.6	...	...	...	...	...	...	0.01	≤ 0.02, ≤ 0.09	...	...

where $n_H(z) \approx n_{H\,I}(z)$ is the total hydrogen density, and $\varphi(z) \equiv n_{Ti\,II}(z)/n_H(z)$ is essentially the fractional abundance of titanium. In terms of the parameters introduced above, $\varphi \approx \delta_{Ti} A_{Ti}$. With independent estimates available for $n_H(z)$, the observed ratio of the column densities of Ti II and H I in Table 2 can be used to constrain the unknown variation of depletion with height through equation (2), which in principle then becomes an equation for $\varphi(z)$.

The first step in the analysis is to consider a choice of model for $n_{H\,I}(z)$. Although the data are as yet extremely limited, the distribution of H I gas above the plane may be described preliminarily by an exponential function,

$$n_{H\,I}(z) = n_0 \exp(-|z|/h_H), \tag{3}$$

where n_0 is the density in the plane, and h_H is the scale height. Recent estimates of the latter range from 500 pc (Bohlin, Savage, and Drake 1978) to 900 pc (HMAL). For the present purpose of using equation (2) to constrain $\varphi(z)$, equation (3) will be adopted as a suitable parametric form for $n_H(z) \approx n_{H\,I}(z)$.

The present data for N(Ti II)/N(H I) are so sparse as to allow a wide range of trial depletion functions $\varphi(z)$. Two particularly simple forms will be investigated, both of which will lead to observable distributions of the general form

$$\frac{N_{Ti\,II}}{N_{H\,I}}(z) = \varphi_0 + \varphi_1 g(z), \tag{4}$$

where the monotonic function $g(z)$ has the properties $0 \le g(z) \le 1$, $g(0) = 0$, and $g(\infty) = 1$. Since the value of the parameter φ_0, the ratio of $N_{Ti\,II}$ to $N_{H\,I}$ at $z = 0$, can be already fixed at 0.55×10^{-9} from the observations of Stokes (1978) in the plane, the essential distinction among the candidate depletion functions lies in the amplitudes φ_1 and the shapes $g(z)$ which they, respectively, yield in equation (4) for the halo.

Perhaps the simplest trial form of this kind is the linear, one-parameter choice

$$\varphi(z;\varphi_1) = \varphi_0 + \varphi_1 z/h_H, \tag{5a}$$

where φ_1 is a free parameter. A substitution of equations (3) and (5a) into equation (2) indeed does yield equation (4), with the particular form

$$g(z) = \left[1 - \left(1 + \frac{z}{h_H}\right)\exp\left(-\frac{z}{h_H}\right)\right] \Big/ \left[1 - \exp\left(-\frac{z}{h_H}\right)\right]. \tag{5b}$$

More complicated depletion functions can of course be chosen, and a useful example of a nonlinear, two-parameter form, with the desired properties, is given by

$$\varphi(z;\varphi_1, h_D) = \varphi_0 + \varphi_1\left[1 - \exp\left(-\frac{z}{h_D}\right)\right], \tag{6a}$$

where ϕ_1 and the depletion scale height h_D are free parameters. The substitutions analogous to those noted above again lead to equation (4), but now with the particular form

$$g(z;h_R) = 1 - \frac{h_R}{h_H}\left[1 - \exp\left(-\frac{z}{h_R}\right)\right] \Big/ \left[1 - \exp\left(-\frac{z}{h_H}\right)\right], \tag{6b}$$

where

$$h_R \equiv h_H h_D/(h_H + h_D) \tag{6c}$$

is the reduced scale height.

Figure 9 compares these two depletion models encompassed by equations (5) and (6) with the observed column density ratios, by virtue of equation (4). Figure 9*a* plots the least squares fit of a linear depletion function to the observed points, calculated with the two different choices $h_H = 500$ and 900 pc, while Figure 9*b* plots the least squares fit of an exponential depletion function with the two choices for each of h_H and h_D set to 500 and 900 pc. It is clear that neither theoretical model is an adequate representation of the observations below $|z| \sim 200$ pc. This systematic effect most likely suggests the presence at $|z| \lesssim 200$ pc of a "two-component" distribution of disk and halo (i.e., $\varphi = \varphi_{disk} + \varphi_{halo}$), as opposed to the one-component halo distribution studied here. However, these trial depletion functions are intended only to describe the halo over scale lengths on the order of a kiloparsec, since neither are there sufficient data nor is it the primary purpose of this study to analyze the galactic disk. Accordingly, in Figure 10, the halo abundances have been "corrected" for disk absorption along the line of sight by subtracting, for both the Ti II and H I, the column densities arising in the velocity range over which absorption occurs toward the foreground star. The format of Figure 10 is the same as that of Figure 9. It would of course be preferable to subtract directly the foreground and background column densities, but this requires H I absorption measurements which are likely to remain generally unavail-

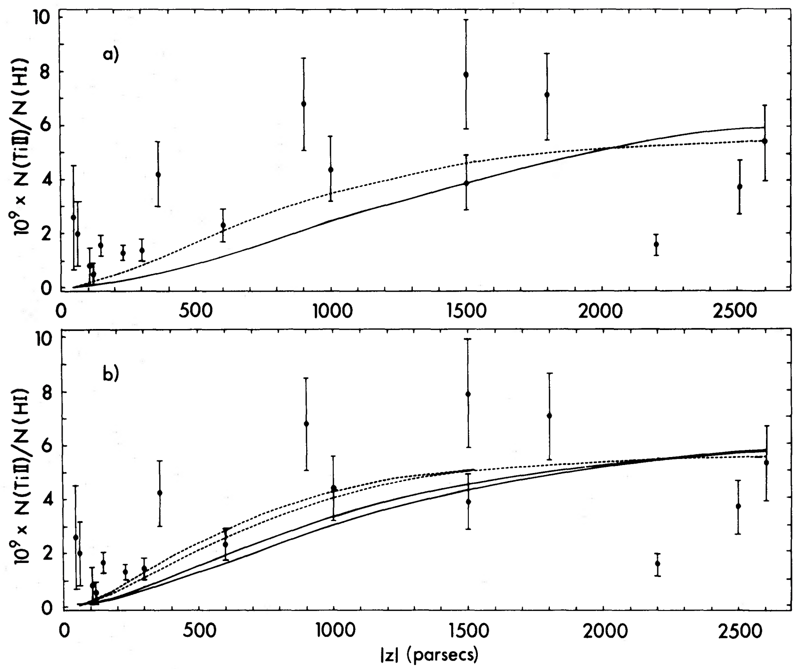

FIG. 9.—The observed total titanium abundances above the galactic plane. Figure 9*a* plots the least squares fit of a linear depletion function to the observed points, calculated with the two different choices for the H I scale height of 500 pc (*dashed line*) and 900 pc (*solid line*). Figure 9*b* plots the least squares fit of an exponential depletion function to the observed points with the two different choices for both the H I and the depletion scale heights of 500 and 900 pc. *Upper dashed line*, $(h_H, h_D) = (500,500)$; *lower dashed line*, $(h_H, h_D) = (500,900)$; *upper solid line*, $(h_H, h_D) = (900,500)$; *lower solid line*, $(h_H, h_D) = (900,900)$. The depletion models are discussed in § IV*b*. The rms uncertainty in each column density ratio is shown by an error bar, while uncertainties in the *z*-distances may be about 20%.

able toward the foreground stars of later spectral type. The adopted technique, which effectively considers only the gas at $|v| > 10$ km s^{-1}, actually overcorrects the halo absorption for the existence of a disk for two reasons: first, Figure 6 shows that, along seven out of nine disk-halo lines of sight, approximately 50%–90% of the absorption does occur beyond the foreground star, and second, Figure 7 implies that subtracting the low-velocity ranges could eliminate up to three-fourths of the halo gas itself.

With the limited data presently available, it is not possible to distinguish between the best fit linear (eq. [5a]) and exponential (eq. [6a]) depletion functions used to model the titanium abundances in Figures 9 and 10. However, these two figures may exemplify limits to the actual abundance changes with *z*, suggesting that fractional titanium abundances in the galactic halo may range from about 15 to 40 times the mean value $\varphi_0 = 0.55 \times 10^{-9}$ in the disk, approaching the solar abundances to within a factor of about 3. If abundance variation are due to grain disruption, such large increases in the gas phase abundance must imply nearly complete distruction of at least those parts of the grains which contained most of this particular heavy element.

c) The Ca II *and* Na I *Abundance Ratios*

The physical conditions in the low- and high-velocity components of the interstellar gas above the galactic plane can be investigated by plotting the column density ratios $N(\text{Ca II})/N(\text{Ti II})$ and $N(\text{Ca II})/N(\text{Na I})$ with z (Figs. 11 and 12). Estimates of the ionization balances of these elements (Herbig 1968; Hobbs 1974; Jura 1975; Stokes and Hobbs 1976) yield the expressions

$$\frac{N(\text{Ca II})}{N(\text{Ti II})} = \frac{\delta(\text{Ca})A(\text{Ca})}{\delta(\text{Ti})A(\text{Ti})}\left[\frac{\beta(\text{Ca})}{n_e} + 1\right]^{-1}, \tag{7a}$$

$$\frac{N(\text{Ca II})}{N(\text{Na I})} = \frac{\delta(\text{Ca})A(\text{Ca})}{\delta(\text{Na})A(\text{Na})}\,\frac{[\beta(\text{Na})/n_e + 1]}{[\beta(\text{Ca})/n_e + 1]}, \tag{7b}$$

where $\delta(\text{X})$ is the gas phase abundance of element X as previously defined, $A(\text{X})$ is the solar abundance of element X, $\beta(\text{X}) \equiv \Gamma/\alpha$ is the ratio of the photoionization coefficient of the observed species to the radiative recombination coefficient of the next higher ionization stage, and n_e is the electron density.

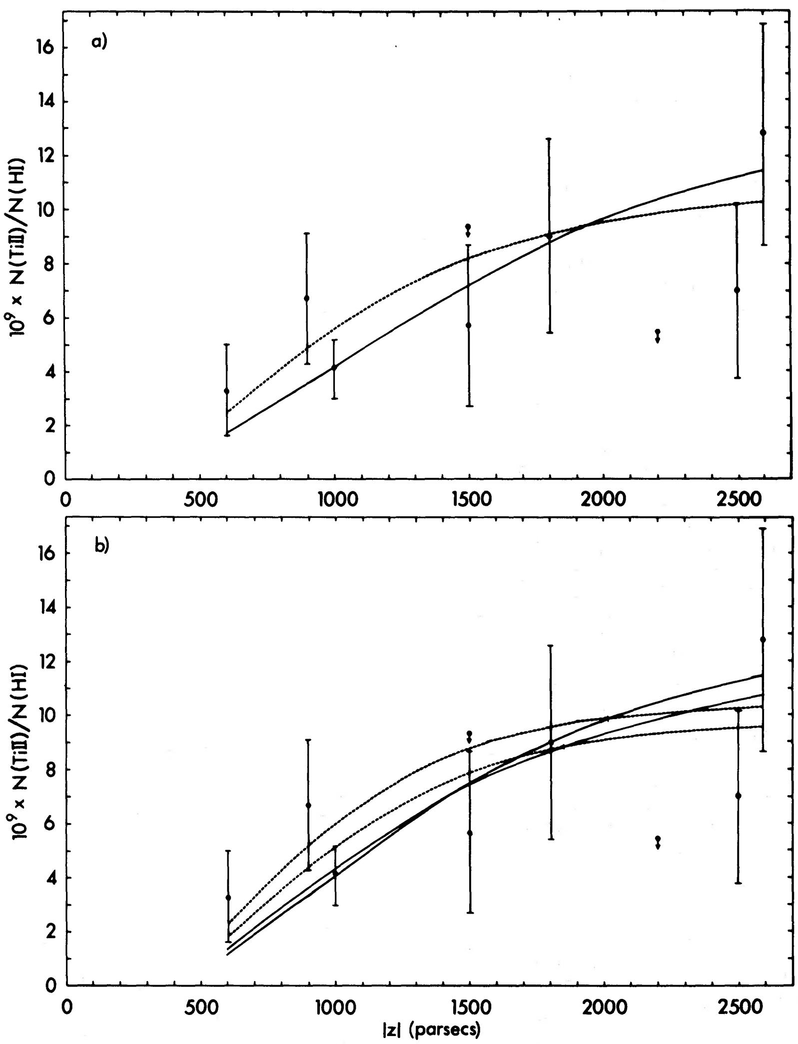

FIG. 10.—The total titanium abundances toward stars of $|z| > 500$ pc, "corrected" (§ IV*b*) for disk absorption along the lines of sight. The depletion models and observational uncertainties are computed and plotted as in Fig. 9.

The approximate invariance of the observed ratio $N(\text{Ca II})/N(\text{Ti II})$ in Figure 5 suggests that the ratio of the gas phase abundances of calcium and titanium, $\delta(\text{Ca})/\delta(\text{Ti})$, is roughly constant, in agreement with Stokes's (1978) result in the disk. Therefore, its similar invariance in Figures 11*a* and 11*b* further suggests that the quantity $\beta(\text{Ca})/n_e$, which governs the ionization balance of calcium, also remains roughly constant with z in both velocity regimes. The observed ratio of the two "recombination" species $N(\text{Ca II})/N(\text{Na I})$, which is approximately independent of n_e, thus depends here, in general, on the two quantities $\delta(\text{Ca})/\delta(\text{Na})$ and $\beta(\text{Na})$. Figure 12*b* shows that this ratio remains relatively low for the low-velocity gas but, for the high-velocity gas depicted in Figure 12*a*, is much higher and perhaps appears to increase with height above the plane. While it is possible that, under some conditions, $\beta(\text{Na})$ could strongly increase relative to $\beta(\text{Ca})$ with z-distance, it is much more likely that this plot reflects a change primarily in $\delta(\text{Ca})/\delta(\text{Na})$ with velocity and with z. Figure 13 emphasizes the velocity dependence by plotting the column density ratio $N(\text{Ca II})/N(\text{Na I})$ for individual kinematic components: absorption produced below the foreground stars is subtracted from the corresponding halo lines of sight, denoted by circles, and the foreground disk absorption is shown by triangles. The general characteristics of such a plot in the galactic plane, where $N(\text{Ca II})/N(\text{Na I})$ increases with increasing LSR velocity, are well known (Routly and Spitzer 1952; Siluk and Silk 1974). In Figure 13, the low-velocity gas in the disk and that in the halo behave comparably, with $N(\text{Ca II})/N(\text{Na I})$ generally ≤ 1 (with five interesting

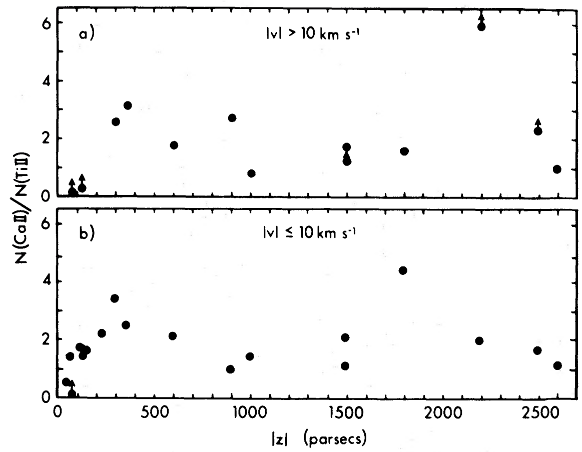

FIG. 11.—The ratio of the total column densities of Ti II and Ca II observed in the two velocity ranges $|v| > 10$ km s^{-1} and $|v| \leq 10$ km s^{-1} above the galactic plane. The rms errors in the column density ratio average 0.37, while uncertainties in the z-distances may be about 20%.

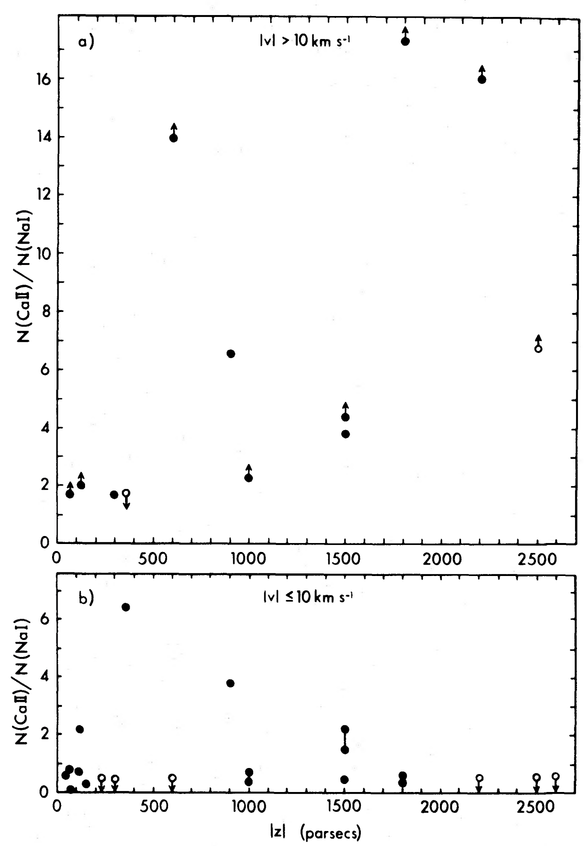

FIG. 12.—The ratio of the total column densities of Ca II and Na I observed in the two velocity ranges $|v| > 10$ km s^{-1} and $|v| \leq 10$ km s^{-1} above the galactic plane. Since the Na I absorption lines are frequently either saturated (*open circles*) or reported as upper limits, errors in the column density ratio vary widely (Table 3), while uncertainties in the z-distances may be about 20%.

cases, along three lines of sight, of low-velocity halo gas with a high calcium to sodium ratio). In contrast, while the column density ratio varies widely in the high-velocity halo gas, it is always ≥ 1.5. Detailed studies of similar correlations in the ultraviolet line ratios of the "dominant-depleted" (cf. Stokes 1978) ions Fe II and Si II to "dominant-cosmic" S II (Shull, York, and Hobbs 1977) demonstrate that the increasing calcium to sodium ratio is probably due to the large gas phase abundance of calcium caused by disruption of interstellar grains. More importantly, this conclusion is demonstrated directly for Ti II in the present set of observations by the corresponding increase of the observed titanium abundances, N(Ti II)/N(H I), with velocity (Fig. 14).

In principle, the electron densities of the observed gas can be estimated from the ratio of Ti II and Ca II column densities with the method developed by Stokes and Hobbs (1976). This method is based on the assumption that variations in the ratio $R = N(\mathrm{Ca})/N(\mathrm{Ti})$ of the total gas phase abundances of calcium and titanium can be neglected in comparison with those in n_e, and R is calibrated with independent measurements of n_e from observations of the Ca I/Ca II line ratio along eight lines of sight in the disk. Since R has not been so calibrated in the halo, n_e remains undetermined. Nonetheless, Figure 5 indicates that ionization conditions in the observed gas are probably not greatly different from those in the plane. As expected, the interstellar radiation field in the lower halo is most likely dominated by stars in the disk.

Thus, it is primarily variations in the abundances and not in the ionization balances above the galactic plane that control the observed column density ratios of Ca II and Na I in the present limited data sample.

V. FURTHER CONCLUSIONS

The primary result of this study is a synthesized picture of the cool neutral interstellar gas in the lower galactic halo. This gas consists of two different types with distinct distribution, kinematics, and abundances: a thick, low-velocity disk (type A) extending from the plane to well beyond the thin disk of OB stars, and high-velocity, much less strongly depleted gas (type B) observed only at high z-distances. The relatively great strength in the type B gas of the absorption lines of Ti II and Ca II, two elements which usually are severely depleted from the type A gas in the disk, compared with the absorption lines of Na I, a usually nearly undepleted element, is explained as only a deficiency of grains in the type B gas; the 21 cm profiles show that the total column densities and therefore masses of the two types of neutral gas in the lower halo near the solar circle are not widely different.

The implications of this model can be considered in terms of the possible origins of the observed high-z gas and in its comparison with QSO absorption lines.

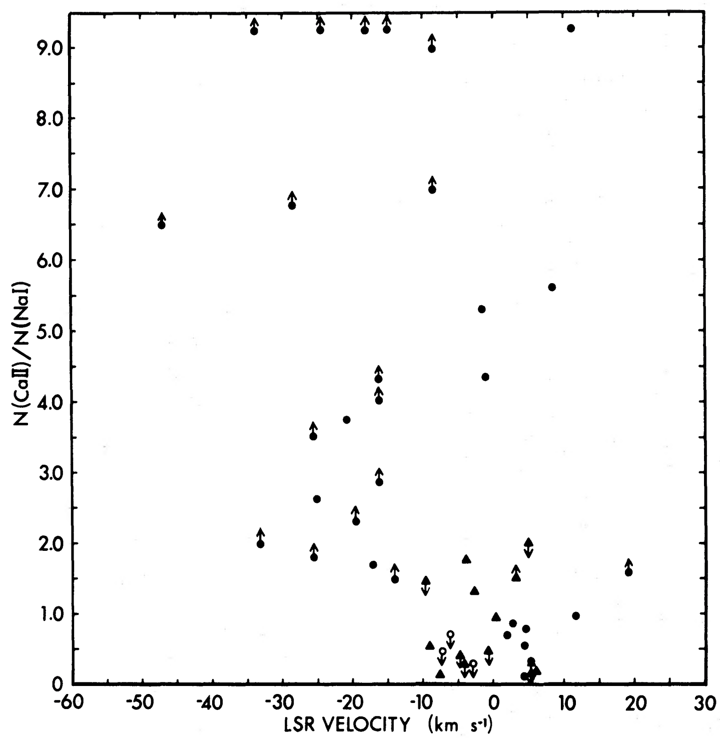

FIG. 13.—The ratio of the column densities of Ca II and Na I observed for individual kinematic components. The column densities produced below the foreground stars have been subtracted from the corresponding halo lines of sight, which are denoted by circles. Open circles denote saturated components. The foreground disk absorption is shown by triangles. The uncertainties in the column density ratio are as in Fig. 12.

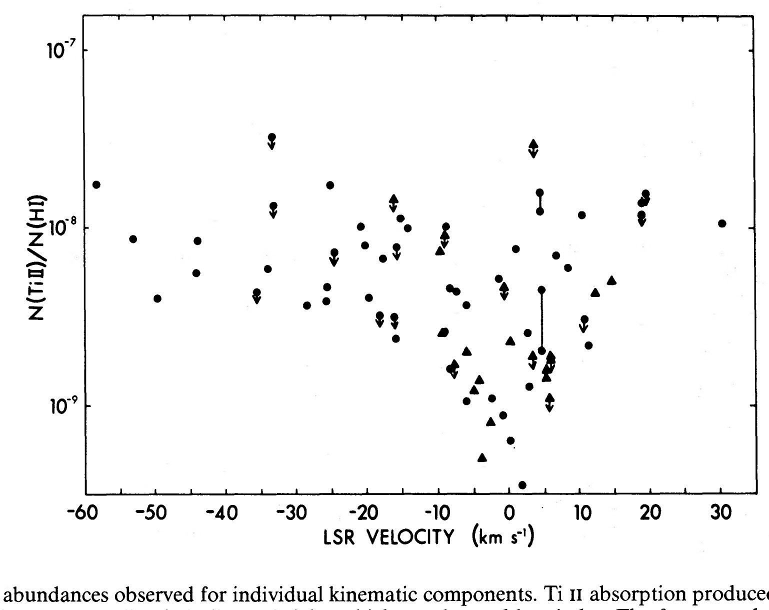

FIG. 14.—The titanium abundances observed for individual kinematic components. Ti II absorption produced below the foreground stars has been subtracted from the corresponding halo lines of sight, which are denoted by circles. The foreground disk absorption is shown by triangles. Since the H I emission is produced by material along the entire line of sight, these column density ratios are lower limits to the actual titanium abundances. The rms errors in the individual titanium abundances average 1.2×10^{-9}.

a) *Possible Origins of High-z Gas*

The observations reveal some basic characteristics of the motions of high-z gas that can be compared with theoretical models of the lower halo. Figure 4 demonstrates that the velocity ranges of the Ti II and Ca II absorption are biased toward negative velocities with respect to the local standard of rest. This trend was initially observed in interstellar Ca II absorption toward high-latitude stars within a galactic longitude range of 80°–185° by Cohen and Meloy (1975), although the negative velocity offset was well within the formal uncertainty in their velocity scale. As expected for the low-velocity type A gas, Ti II line components observed toward the foreground stars have a mean velocity of -0.8 km s^{-1} and a velocity dispersion of 7.9 km s^{-1}, comparable to interstellar clouds in the disk. In contrast, the mean velocity of Ti II components beyond the foreground stars, which includes type B gas, is -9.6 km s^{-1}, and the velocity dispersion is 19 km s^{-1}. However, owing to its highly variable depletion, Ti II is not necessarily a reliable tracer of the kinematics of the bulk of the interstellar hydrogen gas. The velocity distribution of the H I gas itself is shown directly in Figure 15, which plots the average value, for all lines of sight, of the fraction of the total H I column density observed within 10 km s^{-1} velocity bins. In spite of the disk contamination inherent in the 21 cm emission observations, the velocity distribution of the interstellar gas is predominantly negative with respect to the local standard of rest. Since the overall velocity distributions of Ti II and H I here are indeed similar, it can be inferred that, like the high-velocity Ti II depicted in Figure 7, the high-velocity H I gas is most probably located above the foreground disk stars. This gas is evidently characterized by a higher gaseous abundance of Ti II (Fig. 14) and Ca II (Fig. 13).

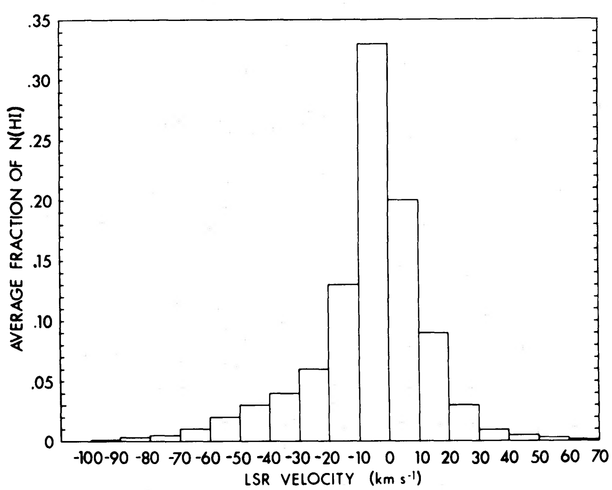

FIG. 15.—The velocity distribution of H I gas above the galactic plane. The average value, for all lines of sight, of the fraction of the total H I column density within 10 km s^{-1} velocity bins is calculated.

A simple kinematic model that has been invoked frequently is that of a gaseous halo corotating with the galactic disk. It is possible to compare the velocity ranges of the observed interstellar absorption of the present study with those expected from such a model halo. Since the projected galactocentric distances of these high-latitude stars range only from 8.1 to 11.0 kpc, the rotation-velocity curve was approximated by a simple power law (Mihalas and Routly 1968) with standard solar values $R_0 = 10$ kpc and $\theta_0 = 250$ km s^{-1}. Alternate choices of a flat rotation curve and solar values $R_0 = 8.5$ kpc and $\theta_0 = 220$ km s^{-1} result in differences of only 3–4 km s^{-1} in the predicted corotation velocity ranges toward these stars. In Figure 4, the thin lines under each bar correspond to the velocity range predicted for corotating material along each line of sight. It is clear that the interstellar Ti II and Ca II observed toward all of these stars exhibit large peculiar velocities with respect to a corotating halo.

The predicted velocity ranges are also compared with the 21 cm emission profiles in Figure 2, where they are indicated by brackets directly above each H I velocity axis. Toward the high-z star of each pair, an average of 69% of the total H I emission is produced by gas at velocities outside the corotation range. If the gaseous halo does indeed rotate with the disk, then there is evidently a significant amount of gas whose motions are controlled, in addition, by large peculiar velocities. Figure 16 illustrates the distribution of these peculiar velocities with respect to the predicted corotation range, plotting the average value, for all lines of sight, of the fraction of the total H I column density observed within 10 km s^{-1} bins centered outside the predicted velocity range. This histogram depicts the observed velocity distribution, making no attempt to portray the fractional mass of gas at various velocities. It actually represents a lower limit to the peculiar velocity distribution, since peculiar velocities can also serve to redistribute gas only within the corotation ranges (1–24 km s^{-1} wide). The velocity distribution is again seen to be skewed toward negative peculiar velocities, now further measured with respect to this particular model of halo rotation.

Alternatives to a corotating galactic halo have been proposed recently. Both theoretical arguments (Sawa and Fujimoto 1980) and observations of H I emission and ultraviolet absorption lines (de Boer and Savage 1983) indicate that the gaseous halo may be rotating more slowly than the disk. If the halo is rotating as a solid body at 75 km s^{-1}, as proposed by Sawa and Fujimoto, the predicted velocity ranges along the lines

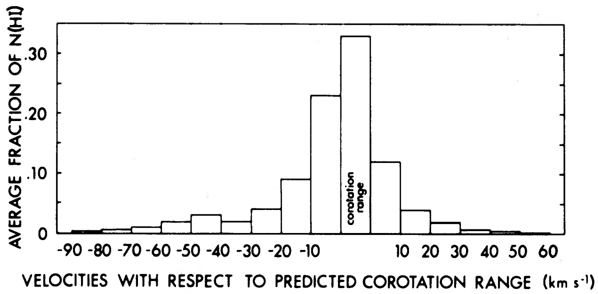

FIG. 16.—The distribution of the peculiar velocities of the H I gas above the galactic plane with respect to the velocity ranges predicted for a corotating halo. The average value, for all lines of sight, of the fraction of total H I column density is calculated within 10 km s^{-1} velocity bins centered outside the predicted corotation range.

of sight to most of the stars of the present study would extend to velocities at least as high as -50 km s^{-1} and, in some cases, up to -125 km s^{-1}. Although this is more consistent with the observed velocity distribution, the predicted ranges depend so sensitively on the exact choice of model that the limited number of lines of sight currently observed is insufficient to constrain possible halo parameters. Further, hydrodynamic considerations of the viscous coupling between interstellar gas in a disk and slowly rotating halo (Waxman 1978) may give rise to circulation currents themselves capable of mixing the gas within several scale heights of the galactic plane on a time scale of about a billion years. The present observations may be qualitatively compatible with such a large-scale circulation pattern.

These observations also appear to be generally consistent with a thick extended disk intermixed at high z-distance with material from a galactic fountain in a hot corona, generally of the type described by Spitzer (1956; Shapiro and Field 1976; Chevalier and Oegerle 1979). The velocity distribution of clouds which are radiatively cooling and condensing in such a fountain would be expected to be skewed toward negative infall velocities (Bregman 1980*b*). As discussed in § III*b*, at least 24% of the total observed halo gas is at high (>10 km s^{-1}) velocities, which, on this model, sets a lower limit on the amount of material participating in a galactic fountain. The negative velocities observed are consistent with the free fall velocities predicted by Bregman (1980*b*) for clouds which form about 1–2 kpc above the plane, and the higher gaseous abundance of Ti II and Ca II in the type B gas could be produced by the disruption of interstellar grains in the galactic fountain. Since no high-velocity clouds are observed toward the foreground stars, the fountain material must merge with the low-velocity extended disk at z-distances beyond those of the foreground stars. Such mixing could be responsible for the observation (Table 6) that, although the Ti II gaseous abundance toward the foreground stars is lower than that toward the background high-z stars, it is still somewhat higher than the mean value in the disk. If the fountain picture is correct, the present observations of interstellar gas above the galactic plane can be represented by a superposition of material of two different origins: type B gas is high-z galactic fountain material which accelerates from initially low velocities to high negative infall velocities as it nears the disk, while the low-velocity gas observed in absorption beyond the foreground stars could represent both type A material and clouds near their turning points at the top of the galactic fountain, which have not yet significantly fallen after forming (Bregman 1980*b*).

Gas observed in the galactic halo may also originate from the infall of intracluster material of the Local Group into the gravitational potential well of our Galaxy (Oort 1966; Cox and Smith 1976; Weisheit and Collins 1976). This suggestion is qualitatively constrained by the present observations that the total abundances of heavy elements such as titanium and calcium in the type B gas and dust probably are nearly solar; it is "processed" or "enriched" matter.

The possible relation between the observed type B gas and the well-known "high-velocity clouds" (generally defined as $|v| \geq 100$ km s^{-1}) observed in 21 cm surveys is not entirely clear. The most comprehensive survey of high-velocity neutral hydrogen (Giovanelli 1980) includes observations near the positions of seven of the nine program stars, and detections are reported within $\Delta l \leq 2°$ and $\Delta b \leq 7°$ of the stellar positions for HD 93521, 97991, 215733, 219188, and 220172. Wesselius and Fejes (1973) discussed observations of intermediate negative-velocity gas ($-91 < v < -21$ km s^{-1}) from the Groningen High Latitude Survey and listed detections, within the same limits, of the positions of HD 93521, 97991, and 215733. Although several models have been suggested, including infall (Oort 1966) and a galactic fountain (Bregman 1980*b*), it is perhaps most likely that a range of phenomena are represented in the 21 cm high-velocity clouds.

b) *Comparison with QSO Absorption Lines*

It is important not only to study the basic structure of our own Galaxy outside the readily visible disk, but also to ask whether our gaseous halo is typical of galaxies in general. This question, recently reviewed by York (1982), is prompted by numerous observations of absorption-line systems appearing at various redshifts in the spectra of distant QSOs, which may be produced by a superposition of intervening galactic halos along each line of sight (Bahcall and Spitzer 1969; Weymann *et al.* 1979; Bregman 1981; Haschick and Burke 1975; Boksenberg and Sargent 1978; Savage and Jeske 1981).

TABLE 7

Ca II Absorption toward Extragalactic Objects

Object	W_λ(K) (mÅ)	Reference
Galactic Ca II		
LMC	150	Songaila 1981*b*
LMC	60	Blades 1980
LMC	50	Walborn 1980
NGC 4321	165	Penston and Blades 1980
NGC 1316	210	Blades 1981
NGC 1068	350	Richstone and Morton 1975
NGC 1058	350	Greenstein 1968
Fairall 9	135	Songaila 1981*a*
Markarian 509	200	York *et al.* 1982
3C 273	$\lesssim$ 500?	Greenstein 1968
3C 273	220	Carswell *et al.* 1979
3C 273	215	Cowie, Songaila, and York 1981
3C 232	200	Boksenberg and Sargent 1978
PKS 2020-370	320	Boksenberg *et al.* 1980
Extragalactic Ca II		
NGC 5253	190	Wallerstein *et al.* 1972
NGC 4321	355	Penston and Blades 1980
NGC 1316	70	Blades 1981
NGC 3067	430	Boksenberg and Sargent 1978
A, B Klemola 31	350	Boksenberg *et al.* 1980
ANON	960	Blades *et al.* 1980

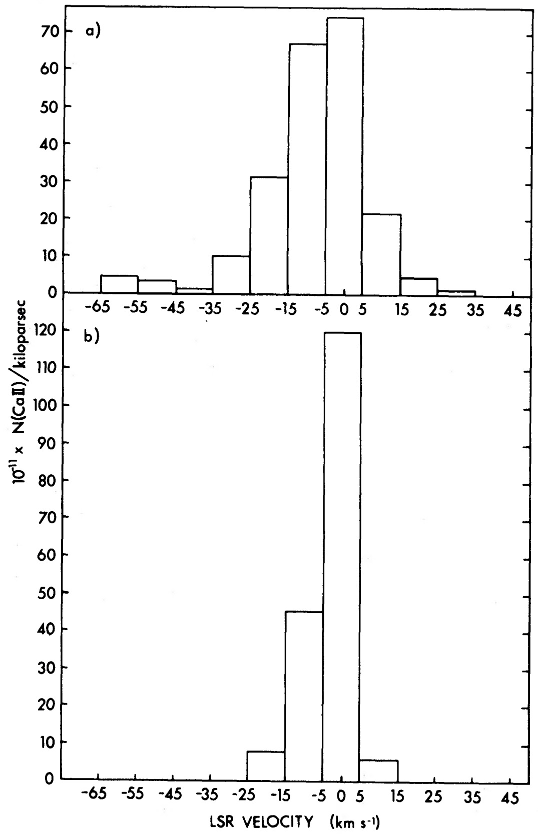

FIG. 17.—A "composite" Ca II profile, as discussed in the text (§ V*b*), that might be seen by an outside observer looking through our Galaxy at the solar circle. Figure 17*b* depicts the "composite profile" produced along the lines of sight toward the foreground stars ($|z| < 300$ pc), while Figure 17*a* shows the corresponding profile produced toward the background stars ($|z| > 300$ pc).

The comparison of optical observations of our galactic halo with others is confined, by the detection limit presently achievable toward QSOs, to essentially the strong absorption lines of the K line of Ca II. Accordingly, the Ca II absorption lines of the present study can be compared with extragalactic Ca II absorption in terms of the general integrated properties of total equivalent width and total line profile. Table 7 lists measurements of the total equivalent width of Ca II absorption, both of our own galactic halo as seen in its entirety toward extragalactic sources, and of other galaxies. The line strengths of the galactic Ca II in the first part of the Table are similar to the total equivalent widths produced in the lower halo toward the stars of Table 2 with $0.5 < z < 2.5$ kpc. Evidently, Ca II absorption is produced almost entirely in the first 1 to 2 kpc above the galactic plane. These total galactic equivalent widths are also generally comparable to the extragalactic Ca II absorption included in the second part of Table 7.

Although little detailed analysis has yet been possible of the low-resolution QSO absorption-line profiles, they are probably asymmetric blends of many narrow line components (Lowrence *et al.* 1972; Boksenberg, Carswell, and Sargent 1979; Savage and Jeske 1981).

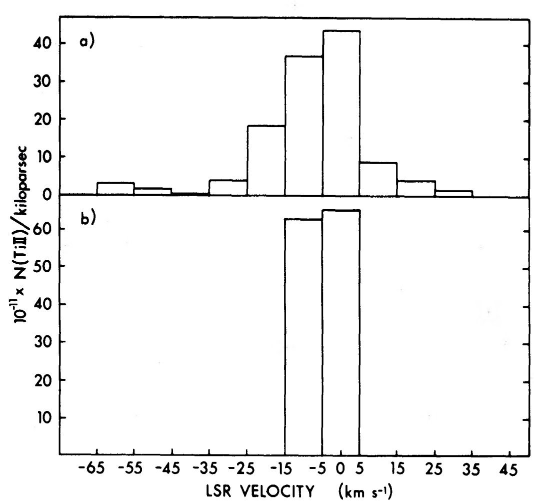

FIG. 18.—A "composite" Ti II profile, as in Fig. 17

Figure 17 illustrates a Ca II "composite profile" that might be seen by an outside observer looking through our Galaxy at the Sun's distance from the galactic center, if the present observations are typical of the interstellar gas along such a line of sight. In this figure, the column density in 10 km s^{-1} velocity bins toward each star has been normalized by the distance to that star and summed for the 19 stars observed. The shape of the resulting density distribution should roughly represent the blended line profile that would be produced along a line of sight through this region of our Galaxy. Figure 17*b* depicts the "composite profile" calculated from the observed Ca II column densities toward the foreground stars of $|z| < 300$ pc, while Figure 17*a* shows the corresponding profile toward the background halo stars. It seems clear that, in galaxies similar to our own, asymmetric absorption-line profiles extending over velocity ranges ≥ 100 km s^{-1} contain high-velocity absorption characteristic of type B halo gas. Such wide profiles are produced by the increasing gas phase abundance at high z and high velocity of elements such as Ca II and Ti II which, in contrast, are generally heavily depleted in the disk. Although the absorption-line strengths of Ti II are well below current detection limits toward QSOs, Figure 18 shows the similar "composite profile" expected for this "dominant" ion.

It is a pleasure to extend my gratitude and appreciation to Dr. L. M. Hobbs for his generous guidance and continuing assistance throughout the course of this work. My sincere thanks are also due to Dr. W. W. Morgan, Dr. Felix J. Lockman, and D. Welty for their contributions to this project, to Drs. K. Cudworth, R. Kron, P. Vandervoort, and D. York for valuable discussions, and to Dr. D. Harper, Dr. R. Loewenstein, R. Dreiser, J. Lola, J. Brooks, J. Draeger, S. Swanson, and, particularly, M. Ertel for their assistance. I would also like to thank the staff of McDonald Observatory for their hospitality and the National Aeronautics and Space Administration for financial support through grant NGR 14-001-147 to L. M. Hobbs.

REFERENCES

Albert, C. E. 1982, *Ap. J. (Letters)*, **256**, L9 (Paper I).
Bahcall, J. N., and Spitzer, L. 1969, *Ap. J. (Letters)*, **156**, L63.
Bisiacchi, G. F., Carrasco, C., Costero, R., and Firmani, C. 1978, *Rev. Mexicana Astr. Ap.*, **2**, 309.
Blaauw, A. 1963, in *Stars and Stellar Systems*, Vol. **3**, *Basic Astronomical Data*, ed. K. Aa. Strand (Chicago: University of Chicago Press), p. 401.
Black, J. H., Dupree, A. K., Hartmann, L. W., and Raymond, J. C. 1980, *Ap. J.*, **239**, 502.
Blades, J. C. 1980, *M.N.R.A.S.*, **190**, 33.
———. 1981, *M.N.R.A.S.*, **196**, 65P.
Blades, J. C., Hunstead, R. W., and Murdoch, H. S. 1980, *M.N.R.A.S.*, **194**, 669.
Blanco, V. M., Demers, S., Douglass, G. G., and Fitzgerald, M. P. 1968, *Pub. US Naval Obs.*, Vol. 21.
Bohlin, R. C., Savage, B. D., and Drake, J. F. 1978, *Ap. J.*, **224**, 132.
Boksenberg, A., Carswell, R. F., and Sargent, W. L. W. 1979, *Ap. J.*, **227**, 370.
Boksenberg, A., Danziger, I. J., Fosbury, R. A. E., and Goss, W. M. 1980, *Ap. J. (Letters)*, **242**, L145.
Boksenberg, A., and Sargent, W. L. W. 1978, *Ap. J.*, **220**, 42.
Bregman, J. 1980*a*, *Ap. J.*, **237**, 280.
———. 1980*b*, *Ap. J.*, **236**, 577.
———. 1981, *Ap. J.*, **250**, 7.
Caldwell, J. 1979, Ph.D. thesis, Princeton University Observatory.
Carswell, R. F., Morton, D. C., Smith, M. G., and Weymann, R. J. 1979, quoted in Ulrich *et al.* (1980).
Chevalier, R. A., and Oegerle, W. R. 1979, *Ap. J.*, **227**, 398.
Cohen, J. G. 1974, *Ap. J.*, **194**, 37.
Cohen, J. G., and Meloy, D. A. 1975, *Ap. J.*, **198**, 545.
Conti, P. S., and Ebbets, D. 1977, *Ap. J.*, **213**, 438.
Cowie, L. L., Songaila, A., and York, D. G. 1981, *Ap. J.*, **246**, 653.
Cowie, L. L., Taylor, W., and York, D. G. 1981, *Ap. J.*, **248**, 528.
Cowley, A., Cowley, C., Jaschek, M., and Jaschek, C. 1969, *A.J.*, **74**, 375.
Cox, D. P., and Smith, B. W. 1976, *Ap. J.*, **203**, 361.
Cudworth, K. M. 1976*a*, *A.J.*, **81**, 519.
———. 1976*b*, *A.J.*, **81**, 975.
———. 1979*a*, *A.J.*, **84**, 774.
———. 1979*b*, *A.J.*, **84**, 1005.
———. 1979*c*, *A.J.*, **84**, 1312.
Cudworth, K. M. 1979*d*, *A.J.*, **84**, 1866.
de Boer, K. S., and Savage, B. D. 1983; *Ap. J.*, **265**, 210.
Giovanelli, R. 1980, *A.J.*, **85**, 1155.
Greenstein, J. L. 1968, *Ap. J.*, **152**, 431.
Guetter, H. 1974, *Pub. A.S.P.*, **86**, 795.
Habing, H. J. 1969, *Bull. Astr. Inst. Netherlands*, **20**, 177.
Haschick, A. D., and Burke, B. F. 1975, *Ap. J. (Letters)*, **200**, L137.
Herbig, G. H. 1968, *Zs. Ap.*, **68**, 243.
Hill, P. W. 1970, *M.N.R.A.S.*, **150**, 23.
Hobbs, L. M. 1971, *Ap. J.*, **166**, 333.
———. 1974, *Ap. J. (Letters)*, **188**, L107.
———. 1978*a*, *Ap. J. Suppl.*, **38**, 129.
———. 1978*b*, *Ap. J.*, **222**, 491.
Hobbs, L. M., Morgan, W. W., Albert C. E., and Lockman, F. J. 1982, *Ap. J.*, **263**, 690 (HMAL).
Hoffleit, D. 1964, *Catalogue of Bright Stars* (3d ed.; New Haven, Conn.: Yale University Observatory).
Hogg, H. S. 1973, *Pub. David Dunlap Obs.*, Vol. **3**, No. 6.
Johnson, H. L. 1963, in *Stars and Stellar Systems*, Vol. **3**, *Basic Astronomical Data*, ed. K. Aa. Strand (Chicago: University of Chicago Press), p. 214.
Johnson, H. L., Mitchell, R. I., Iriarte, B., and Wiśniewski, W. Z., 1966, *Comm. Lunar and Planet. Lab.*, **4**, 99.
Jura, M. 1975, *Ap. J.*, **200**, 415.
Lesh, J. R. 1968, *Ap. J. Suppl.*, **17**, 371.
Lowrence, J. L., Morton, D. C., Zuchino, P., Oke, J. B., and Schmidt, M. 1972, *Ap. J.*, **171**, 233.
Mihalas, D., and Binney, J. 1981, *Galactic Astronomy* (2d ed.; San Francisco: W. H. Freeman), p. 252.
Mihalas, D., and Routly, P. M. 1968, *Galactic Astronomy* (San Francisco: W. H. Freeman), p. 142.
Morgan, W. W., Abt, H. A., and Tapscott, J. W. 1978, *Revised MK Spectral Atlas for Stars Earlier than the Sun* (private printing).
Morgan, W. W., Code, A. D., and Whitford, A. E. 1955, *Ap. J. Suppl.*, **2**, 41.
Morton, D. C., and Smith, W. H. 1973, *Ap. J. Suppl.*, **26**, 333.
Münch, G., and Zirin, H. 1961, *Ap. J.*, **133**, 11 (MZ).
Nachman, P., and Hobbs, L. M. 1973, *Ap. J.*, **182**, 481.
Oort, J. H. 1966, *Bull. Astr. Inst. Netherlands*, **18**, 421.
Penston, M. V., and Blades, J. C. 1980, *M.N.R.A.S.*, **190**, 51P.
Pettini, M., and West, K. A. 1982, *Ap. J.*, **260**, 561.

Preston, G. W. 1959, *Ap. J.*, **130**, 507.
Ramella, M., Morossi, C., and Santin, P. 1980, *Astr. Ap.*, **90**, 146.
Richstone, D. O., and Morton, D. C. 1975, *Ap. J.*, **201**, 289.
Rickard, J. J. 1972, *Astr. Ap.*, **17**, 425.
Routly, P. M., and Spitzer, L. 1952, *Ap. J.*, **115**, 227.
Sargent, W. L. W., Young, P. J., Boksenberg, A., Carswell, R. F., and Whelan, J. A. J. 1979, *Ap. J.*, **230**, 49.
Savage, B. D., Bohlin, R. C., Drake, J. F., and Budich, W. 1977, *Ap. J.*, **216**, 291.
Savage, B. D., and de Boer, K. S. 1981, *Ap. J.*, **243**, 460.
Savage, B., and Jeske, N. A. 1981, *Ap. J.*, **244**, 768.
Sawa, T., and Fujimoto, M. 1980, *Pub. Astr. Soc. Japan*, **32**, 551.
Shapiro, P. R., and Field, G. B. 1976, *Ap. J.*, **205**, 762.
Shull, J. M., York, D. G., and Hobbs, L. M. 1977, *Ap. J.*, **211**, 803.
Siluk, R. S., and Silk, J. 1974, *Ap. J.*, **192**, 51.
Songaila, A. 1981*a*, *Ap. J.*, **243**, L19.
______. 1981*b*, *Ap. J.*, **248**, 945.
Songaila, A., and York, D. G. 1980, *Ap. J.*, **242**, 976.
Spitzer, L. 1956, *Ap. J.*, **124**, 20.
______. 1978, *Physical Processes in the Interstellar Medium* (New York: Wiley-Interscience), p. 163.
Stokes, G. M. 1978, *Ap. J. Suppl.*, **36**, 115.
Stokes, G. M., and Hobbs, L. M. 1976, *Ap. J.* (*Letters*), **208**, L95.
Strömgren, B. 1948, *Ap. J.*, **108**, 242.
Tobin, W., and Kilkenny, D. 1981, *M.N.R.A.S.*, **194**, 937.
Tull, R. G., Choisser, J. P., and Snow, E. H. 1975, *Appl. Optics*, **14**, 1182.
Uesugi, A., and Fukuda, I. 1970, *Contr. Inst. Ap. and Kwasan Obs., Univ. Kyoto*, No. 189.
Ulrich, M. H., *et al.* 1980, *M.N.R.A.S.*, **192**, 561.
Vidal-Madjar, A., Laurent, C., and Bonnet, R. M. 1977, *Ap. J.*, **211**, 91.
Vogt, S. S., Tull, R. G., and Kelton, P. 1978, *Appl. Optics*, **17**, 574.
Walborn, N. R. 1980, *Ap. J.* (*Letters*), **235**, L101.
______. 1983, *Ap. J.* (*Letters*), **267**, L59.
Wallerstein, G., Conti, P., and Greenstein, J. 1972, *Ap. Letters*, **12**, 101.
Wallerstein, G., and Goldsmith, D. 1974, *Ap. J.*, **187**, 237.
Waxman, A. M. 1978, *Ap. J.*, **222**, 61.
Weisheit, J. C., and Collins, L. A. 1976, *Ap. J.*, **210**, 299.
Wesselius, P. R., and Fejes, I. 1973, *Astr. Ap.*, **24**, 15.
Weymann, R. J., Williams, R. E., Peterson, B. M., and Turnshek, D. A. 1979, *Ap. J.*, **234**, 33.
Williams, D. R. W. 1973, *Astr. Ap. Suppl.*, **8**, 505.
Wilson, R. E. 1953, *General Catalog of Stellar Radial Velocities* (Washington, D.C.: Carnegie Institution of Washington Pub. No. 601).
Withbroe, G. L. 1971, *The Menzel Symposium*, ed. K. B. Gebbie (NBS Spec. Pub. 353).
York, D. G. 1982, *Ann. Rev. Astr. Ap.*, **20**, 221.
______. 1983, *Ap. J.*, **264**, 172.
York, D. G., Blades, J. C., Cowie, L. L., Morton, D. C., Songaila, A., and Wu, C. C. 1982, *Ap. J.*, **255**, 467.
Zinn, R. J., Newell, E. B., and Gibson, J. B. 1972, *Astr. Ap.*, **18**, 390.

C. E. ALBERT: Physics Department, United States Naval Academy, Annapolis, MD 21402